# INFLUENCE OF STATIC AND DYNAMIC TOPOGRAPHY ON OSTEOBLAST PROLIFERATION AND MATURATION

A Dissertation
Presented to
The Academic Faculty

by

Erin Marie Lee

In Partial Fulfillment
of the Requirements for the Degree
Biomedical Engineering in the
Wallace H. Coulter Department of Biomedical Engineering

Georgia Institute of Technology
Emory University
Peking University
December 2016

# INFLUENCE OF STATIC AND DYNAMIC TOPOGRAPHY ON OSTEOBLAST PROLIFERATION AND MATURATION

Approved by:


Dr. Barbara D. Boyan, Advisor
School of Engineering
*Virginia Commonwealth University*

Dr. Johnna Temenoff
Department of Biomedical Engineering
*Georgia Institute of Technology*

Dr. Ken Gall
School of Mechanical Engineering and Materials Science
*Duke University*

Dr. Cheng Zhu
Department of Biomedical Engineering
*Georgia Institute of Technology*

Dr. Haifeng Chen
School of Engineering
*Peking University*

Dr. Ravi Bellamkonda
School of Engineering
*Duke University*


Date Approved: September 16, 2016

# ACKNOWLEDGEMENTS

I wish to thank my family, friends, colleagues, and advisors for their unwavering commitment to my person and my research over the past six years. First to my mother and father, whose support and encouragement throughout my entire life has made such a monumental task attainable. To my brother, Wade, and his daughter Monroe, whose smiling faces brighten any dark laboratory night. To my myriad of aunts, uncles, and cousins who bewilderingly listened as I try to explain what *exactly* it was I was doing in Atlanta, and Richmond, and Beijing, and Richmond, and Atlanta. To my late grandmother Bobbie, whose encouraging words I can still hear in my heart.

I had multiple advisors for nearly every area of my project, but without Dr. Barbara Boyan's expertise, advice, and willingness to take on a student who would intentionally be leaving the lab for an entire year, there would be no dissertation on this topic. And without Dr. Zvi Schwartz's continuous push forward, there would be no conclusion to it. I would like to sincerely thank both of them for their guidance throughout my graduate career. Also a tremendous thanks to my mentor Dr. Kathryn Smith, and her advisor and mine, Dr. Ken Gall, who gave me the tools I needed with respect to materials science, and kept me on track. I would like to thank Dr. Haifeng Chen, who graciously accepted me into his laboratory at Peking University for an entire year, and Dr. Ao's lab in the school of medicine there, whose journal clubs will be remembered even if I could not understand a word of them. Instrumental to my survival on the PKU campus were Hening Wang and Muyang Sun, my friends and enjoyers of

excellent food. I would also like to thank my other committee members, Dr. Bellamkonda, Dr. Temenoff, and Dr. Zhu, for their invaluable input into my research.

I would also like to thank my labmates. Many have come and gone through the Boyan lab throughout my time there, but in particular I would like to thank Sharon Hyzy, lab manager, master of all, savior of many an experiment, tutor, and friend (and by extension a thank you to her adorable pup Hugo). I would also like to thank Alice Cheng, a real motivator and role model to me, though she may not have known it until now. Thank you to the MSE undergraduate Caleb Voelkel for helping with the creation and testing of materials.

Finally, I would like to thank John Lee. He knows why.

# TABLE OF CONTENTS

# LIST OF FIGURES

# LIST OF SYMBOLS AND ABBREVIATIONS

| | |
|---|---|
| A | acid-etched |
| bio-MEMs | biomedical microelectromechanical systems |
| BMP | bone morphogenetic protein |
| BZA | benzyl acrylate |
| BZMA | benzyl methacrylate |
| DDMA | 1,12-dodecanediol dimethacrylate |
| DMA | dynamic mechanical analysis |
| DMPA | 2,2-Dimethoxy-2-phenylacetophenone |
| DSC | differential scanning calorimetry |
| ELISA | enzyme-linked immunosorbent assay |
| $E_r$ | rubbery modulus |
| FGF | fibroblast growth factor |
| GB | grit-blasted |
| LSM | laser scanning microscopy |
| MA | methyl acrylate |
| MMA | methyl methacrylate |
| MSC | mesenchymal stem cell |
| OCN | osteocalcin |
| OPG | osteoprotegerin |
| pA | polymer with acid-etched roughness |
| PBS | phosphate buffered saline |
| PDMS | poly dimethylsiloxane |

| | |
|---|---|
| PEGDMA | polyethylene glycol dimethacrylate |
| pGB | polymer with grit-blasted roughness |
| PI | photoinitiator |
| pPT | polymer with pre-treated roughness |
| PT | pre-treated |
| SEM | scanning electron microscopy |
| SMP | shape-memory polymer |
| TCPS | tissue culture polystyrene |
| $T_d$ | deformation temperature |
| $T_g$ | glass transition temperature |
| TGFβ1 | transforming growth factor β1 |
| Ti | titanium |
| UV | ultraviolet |
| VEGF | vascular endothelial growth factor |
| XPS | x-ray photon spectroscopy |

# SUMMARY

Osseointegration remains a primary concern for implanted devices in patients with risk factors such as diabetes, smoking, age, arthritis, and osteoporosis. Current use of titanium alloys, while successful, comes at a high cost. Cheaper alternatives may exist with polymers for some non-load bearing applications. Advancements in polymer chemistry have yielded a class of smart materials called shape-memory polymers (SMPs), which can change their shape via changes in temperature or mechanical stress. This study follows the creation of one such temperature-sensitive SMP, benzyl acrylate-benzyl methacrylate-1,12-dodecanediol dimethacrylate, which can be compressed to remove all surface topography and at 37˚C shows nearly complete recovery within 8 hours. The examination of pre-osteoblast MG63 cell behavior on these SMPs (with and without compression) by DNA and ELISAs indicates MG63 cells can be 'clued' to proliferate and then to rapidly mature. Similar topography was created on polymers of varied stiffness to determine if there is correlation between substrate stiffness and topography on osteoblast maturation. Overall, this thesis gives insight into potential benefits of SMP use in biomedical applications. In addition, it demonstrates the potential issues concerning the use of polymers to achieve a desired cell response.

# CHAPTER 1

# INTRODUCTION

## 1.1 Motivation

Millions of Americans require implanted orthopaedic implants every year, a number that is only expected to increase [1]. The global market for orthopaedic implants is growing rapidly, with the estimated cost reaching over $46 billion by 2017 [2]. While as a whole orthopaedic implants tend to be success stories, there is particular care that needs to be given to those patients for whom this is not the case. Factors such as age, diabetes, smoking, arthritis, and osteoporosis contribute to implant failures, which lead, in the best-case scenario, to costly, potentially risky revision procedures [3,4]. It is these patients who would benefit the most from improved osseointegration of implanted devices.

## 1.2 Specific Aims

The objective of this thesis was to develop, characterize, and implement a novel shape-changing polymer to understand the dynamic effect of topography on osteoblast differentiation. Our central hypothesis is that smooth topography will allow for increased cellular attachment and proliferation of preosteoblasts, and dynamic roughness will enhance differentiation of both preosteoblasts and mesenchymal stem cells (MSCs) into osteoblasts. This hypothesis is based on previous literature exploring the role of topography and osteoblast differentiation on the current gold standard for

osseointegration, titanium [3, 8, 9]. The overall objective was evaluated by testing our central hypothesis in the following specific aims, summarized in Figure 1.1:

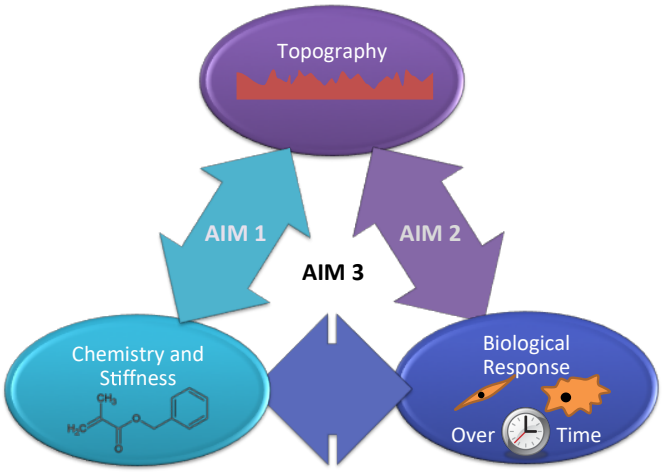


**Figure 1.1**. Relationship of each specific aim in this research

**Specific Aim 1**

Develop and characterize microrough shape-memory polymers that respond to homeostatic temperature. The hypothesis for this aim is that a novel shape-memory polymer network is able to change from smooth to rough topography at homeostatic temperature over varying time courses dependent on monomer concentration. This aim is supported by Chapter 3.

**Specific Aim 2**

Determine if the dynamic recovery of SMPs has an effect on preosteoblast MG63 cell attachment, proliferation, and differentiation into osteoblasts. The hypothesis for this aim is that SMPs with smooth topography will increase cellular attachment and proliferation whereas SMPs with increased roughness will cause increased osteoblastic response. This aim is supported by Chapter 3.

**Specific Aim 3**

Determine if stiffness *and* roughness has an effect on MG63 cell differentiation into osteoblasts. The hypothesis for this aim is that addition of surface roughness to

known MA:MMA polymers at varied stiffnesses will change MG63 response to stiffness. This aim is examined in Chapter 4.

# CHAPTER 2

# BACKGROUND

## 2.1 Shape-Memory Polymers

### 2.1.1 Development

Shape memory polymers (SMPs) have existed in some form or another since the 1960s, when heat-shrink tubing for cables first came about, then in the 1980s they were picked up for automotive use. Polymers, in comparison to metals, are easy to fabricate and resilient in an aqueous environment [5]. SMPs are a class of 'smart' polymers with the ability to change shape via an environmental stimulus, such as temperature, electricity, or mechanical force [6-9]. The polymer can be heated to above its glass transition temperature ($T_g$), compressed or stretched to percent strains in the hundreds, and cooled under such conditions to keep that deformed shape until a time when it receives enough energy to return to its original shape (typically via an increase in temperature). This is true not only for the bulk of the polymer but also for its surface features, down to the nanoscale level [10]. Recovery rates depend on the $T_g$, which is dependent on monomer and crosslinker concentrations, the deformation temperature ($T_d$), and the recovery temperature [11,12].

### 2.1.2 Use in biomedical engineering applications

It wasn't until the 90s and early 2000s that research with SMPs began to wander into the realm of biomedical uses, starting with stents and self-tying sutures [13,14]. Because SMPs can be compressed, twisted, or folded such that their temporary shape can be much smaller than their recovered shape, they are ideal for minimally invasive surgery. SMPs have been studied for blood clot removal [15,16], tooth removal [17], cardiac valves [18], neural probes [19], and biomedical microelectromechanical systems

(bio-MEMS) [20]. As SMPs can be composed of biodegradable polymers, studies have also looked at using them for temporary occlusion [21], and there is to this day still research into self-tying sutures [22].

### 2.1.3 Temperature-sensitive copolymers: structure and synthesis

For this research we have primarily chosen to work with the monomers benzyl acrylate (BZA) and benzyl methacrylate (BZMA) and crosslinker 1,12-dodecanediol dimethacrylate (DDDMA), for a number of reasons. First, polymer networks created from these monomers have excellent toughness, even in an aqueous environment [19]. Second, the only chemical difference between BZA and BZMA is the addition of a methyl group on the second carbon, and while this creates the gap in $T_g$ that allows tailoring around homeostatic temperature (Figure 2.1), it also limits the fluctuations in

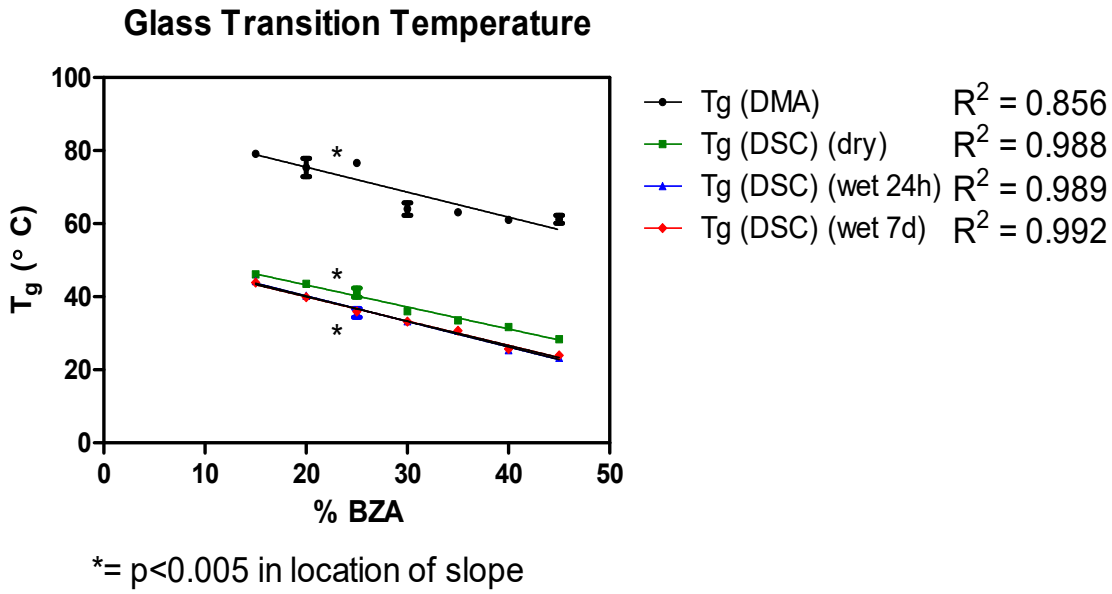


**Figure 2.1**. Effect of BZA concentration and water submersion on glass transition temperature. The increase of benzyl acrylate content decreases the glass transition temperature, the effect of water is to decrease the Tg by two degrees Celsius, and there is no difference in Tg between samples soaked for 24h or 7 days. (n=3)

surface chemistry as the monomer ratio changes. $T_g$ is crucial to an SMP as it directs how well an SMP will maintain its shape at any given temperature, and at which point the SMP begins to recover [6,23]. Finally, the addition of DDDMA as the crosslinker creates

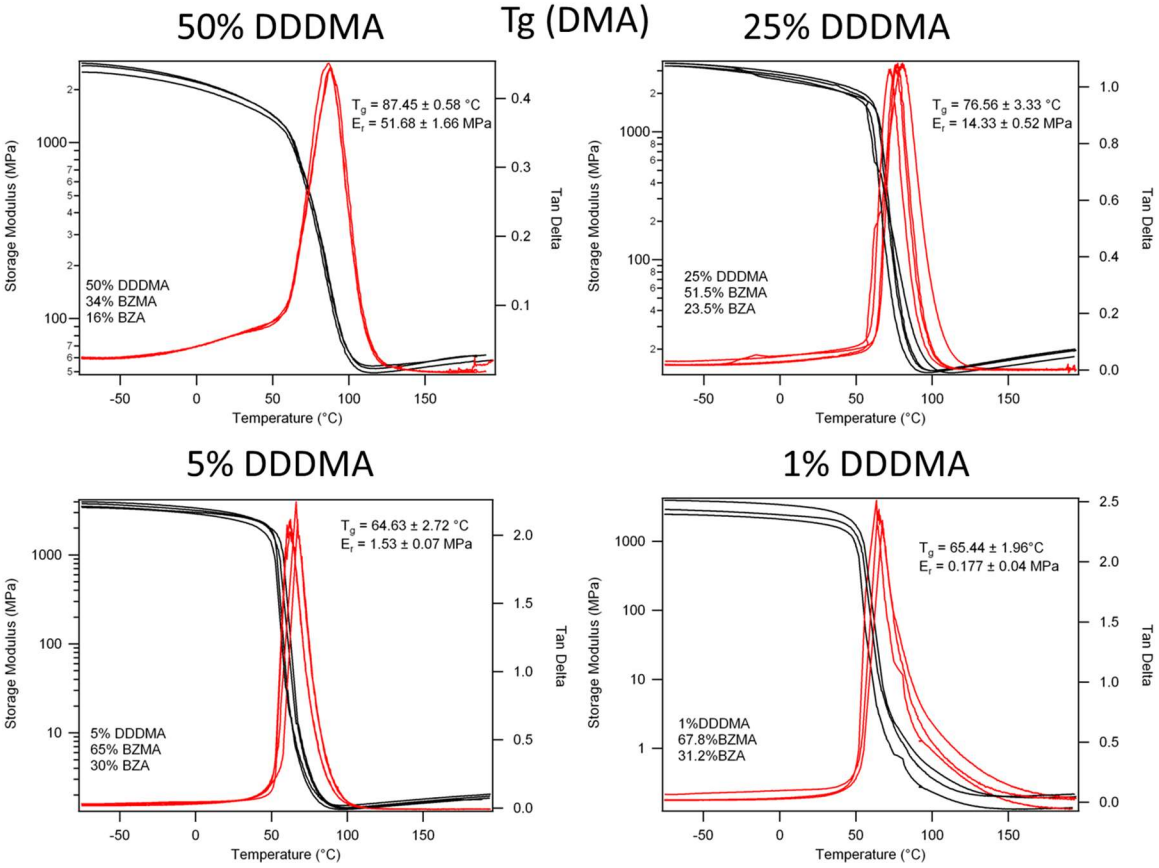


**Figure 2.2**. Effect of crosslinker concentration on glass transition temperature and rubbery modulus. Glass transition temperature was found to be linearly related to % crosslinker and rubbery modulus exponentially related. (n=3)

a network whose rubbery modulus ($E_r$) can be tailored as well, anywhere from 1 to 50 MPa with up to 50% DDDMA (Figure 2.2, see also Figure 3.2). The concentration of crosslinker is also important to an SMP's recovery [11,23]. Ultimately, for a large portion of the studies done a concentration of 30% BZA 65% BZMA and 5% DDDMA was used, as this composition had a $T_g$ close to our target temperature of 37˚C (see Chapter 3).

## 2.2 Osteoblast Differentiation

### 2.2.1 Initial stage

Osteoblasts, or bone-producing cells, begin their journey as MSCs. The complete package as to what drives an MSC towards the osteoblastic lineage is not known, but

what *is* known is that the first stage after lineage commitment is proliferation of pre-osteoblasts, and the upregulation of bone morphogenetic proteins (BMPs), activation of Wnt and Notch signaling, as well as Hedgehog, to produce the transcription factors Runx2 and Osterix [24,25]. During this phase of proliferation, extracellular matrix (ECM) proteins such as type I collagen, fibronectin, and transforming growth factor β (TGFβ) are upregulated [24]. This lays the foundation for the maturation of the matrix and eventual mineralization. Proliferation begins to slow and ultimately stops when further differentiation occurs.

### 2.2.2 Later stages

As the ECM matures, its change helps provide feedback to the cell to further its maturation via the reception of osteopontin and fibronectin, and the cell begins to produce more alkaline phosphatase (ALP) specific activity [24,25]. Next, ALP activity begins to decline and the production of osteocalcin and calcium deposition/accumulation occurs [24]. Finally, an osteoblast reaches terminal differentiation as an osteocyte. This is all in tandem with its counterpart, the osteoclast, which are derived from hematopoetic stem cells.

### 2.2.3 Topographical influence on maturation

Many properties of materials influence cell fate, including surface chemistry and topography, and bulk mechanical and electrical properties [26-30]. While work continues to advance our understanding of the underlying mechanisms of how cells sense their physical, chemical, and mechanical environment, much still remains a mystery. Previous work has shown an inverse correlation of attachment of osteoblast-like cells on increasing microrough titanium surfaces but a positive correlation in differentiation into mature

osteoblasts [4,31,32]. According to these studies, a flatter, smoother topography allows better cell attachment and proliferation while microrough topography allows improved differentiation as indicated by an increase in alkaline phosphatase specific activity, and secreted osteocalcin levels. The incorporation of rough topography has also been shown to increase bone-to-implant contact *in vivo*, which in turn leads to improved osseointegration over smoother topography [33]. However, metal implants are expensive and prone to corrosion, and modification of the surface can change its chemistry, and wettability, drastically. This was another reason why the work here was done via polymers.

# CHAPTER 3

# CHANGE IN SURFACE ROUGHNESS BY DYNAMIC SHAPE-MEMORY ACRYLATE NETWORKS ENHANCES OSTEOBLAST DIFFERENTIATION[1]

## 3.1 Introduction

The cues a cell receives from its external environment, be they mechanical, topographical, or chemical, dictate its fate [30,35]. Studies looking at factors such as surface geometry [27,36], stiffness [26,37], and microstructure [38,39] reinforce the importance of understanding how cells interact with their physical environment. Cells not only sense structural and mechanical cues, but also respond to them by altering their environment through production of extracellular matrix and release of autocrine and paracrine factors. Smart materials use these properties to optimize cellular response, thereby controlling release of bioactive factors [40], creating room for proliferation [41], promoting differentiation of desired phenotypes [42], or causing cells to undergo apoptosis [43].

Microscale surface roughness has been shown to have a significant influence on implant osseointegration as evidenced by increased bone-to-implant contact and pullout strength compared to smooth surfaced implants[44]. In vitro studies indicate that this is

---

[1] Chapter adapted from [34]

due in part to enhanced osteoblast differentiation, demonstrated by an increase of phenotype-specific osteoblast lineage markers [38,39,44,45]. In addition, osteoblasts produce higher levels of osteogenic factors, including bone morphogenetic proteins 2, 4, and 7 (BMP2, BMP4, BMP7) and angiogenic factors, including vascular endothelial growth factor (VEGF) and basic fibroblast growth factor (FGF2), as well as factors that modulate osteoclast activity, including osteoprotegerin (OPG) and transforming growth factor beta-1 (TGFβ1) [4,46-48].

Previous work in our lab and others has shown an inverse correlation between attachment and proliferation of osteoprogenitor cells and increasingly microrough titanium surfaces (that is, as roughness increases attachment decreases); in contrast, there is a positive correlation of surface microroughness with osteoblast differentiation and maturation (that is, as roughness increases, differentiation and maturation increase) [4,31,32]. These observations led us to hypothesize that an ideal osteogenic material would have a smooth surface to ensure adequate initial attachment and proliferation of osteoblast progenitor cells, but provide a time-dependent shift to a microstructured topography to support osteoblast differentiation and maturation. To address this hypothesis, we capitalized on the unique properties of shape-memory polymers (SMPs).

SMPs are a subclass of smart materials that have the ability to "memorize" their original shape through covalent or physical crosslinking. They can be deformed and stored in a temporary shape by heating the polymer beyond its glass transition temperature (Tg), and then cooled back down past their Tg. Various types of triggers can then cause SMPs to recover back to their original shape, including temperature, force, water, or electricity [6-9]. SMPs are being explored for a variety of clinical applications including self-tying

sutures [13], soft tissue fixation, occlusion of aneurysms [49,50], and drug delivery [51]. SMP networks can also exhibit other functionalities including degradability [52-54] or high toughness for use in load-bearing implants [55,56]. These clinical applications leverage the shape memory response to undergo a bulk or macro-scale shape change. There have been few reports of SMPs whose shape recovery is retained at the micro-scale at the material's surface [57].

The objective of this study was to determine if a time-dependent transition from a smooth to rough microtopography would facilitate osteoblast proliferation without negatively impacting the effects of microtexture on differentiation. To do this we developed and characterized an SMP with the mechanical properties that would allow a temporal surface change from smooth to rough under in vitro cell culture conditions and to evaluate effects of its shape memory recovery on osteoblast proliferation and differentiation in comparison to static, microrough surfaces. An acrylate copolymer system was selected that permitted independent tailoring of Tg without varying surface chemistry. Extensive characterization of acrylate monomers in our laboratory identified a number of potential polymer networks with Tg's that could be tuned to body temperature by changing the ratio of monomers and crosslinker [58]. This information, coupled with the observation that MG63 human osteoblast-like cells respond better to particular elastic moduli [37] under certain surface chemistries, led to our identification of benzyl acrylate and benzyl methacrylate as a suitable SMP network to explore mechanisms behind cellular interactions to topographical cues. Rough topographies that mimic those found on clinically-used titanium surfaces were created using soft lithography techniques. The osteogenic response

on these surfaces was assessed in MG63 cells cultured on both static and dynamic SMP networks.

## 3.2 Materials and Methods

### 3.2.1 Material fabrication and synthesis of samples

Benzyl methacrylate (BZMA), benzyl acrylate (BZA), and 1,12-dodecanediol dimethacrylate (DDDMA) were obtained from Sigma-Aldrich (St. Louis, MO) and used as received. 2,2-dimethoxy-2-phenylacetophenone (DMPA, Sigma-Aldrich) was used as the photoinitiator. Dow Corning Sylgard 184 (Fisher Scientific, Pittsburgh, PA) was used to make polydimethylsiloxane (PDMS) molds. Titanium discs with different surface roughnesses were donated by Institut Straumann AG (Basel, Switzerland) and have been described in detail previously [31,59].

PT discs were machined (smooth). In addition, PT discs were either acid etched (A) resulting in a mesoscale texture or were grit blasted (GB) resulting in a microtexture. To fabricate the SMP disks, the base and curing agent from the PDMS kit were mixed at a ratio of 10:1, poured over 15mm PT, A, and GB discs and cured at 150°C for 10 min. At that time, PDMS molds were peeled off and edges were trimmed with a razor blade (Fig. 3.1a-e).

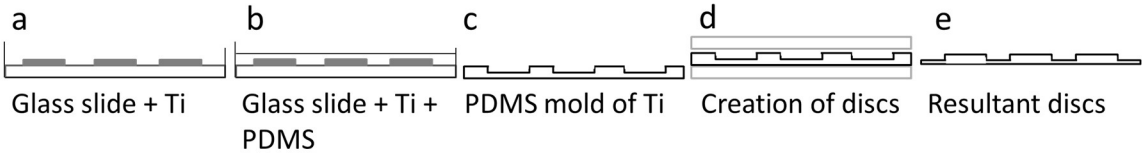


**Figure 3.1** Schematic of disc fabrication. a) Original titanium discs set on glass slide, surrounded by aluminum foil; b) mixed PDMS is poured over the titanium discs and cured at 150 °C for 10 min; c) resultant PDMS mold after peeling and discs are removed; d) PDMS mold in-between glass slides for curing (see methods); e) resultant discs with excess polymer.

Effects of the cross-linker on cell viability were tested using SMP disks fabricated using co-monomer solutions created by combining various weight ratios of DDDMA crosslinker with a 3:6.5 ratio of BZA:BZMA, and 0.5 wt% DMPA. Crosslinker concentrations of 1, 5, 25, and 50 wt%. Based on the results, 5 wt% DDDMA was chosen for subsequent experiments. To fabricate the disks, each solution was mixed manually in a glass vial and injected using a glass pipette between two glass slides separated with two glass spacers (thickness = 1 mm). The sheets were placed in a UV chamber (UVP, Model CL-1000L Ultraviolet Crosslinker, Upland, CA; λ=365 nm; energy = 2000 x 100 μJ/cm2) for 45 min. The glass slides and polymer sheets were post-cured for 90 min at 90°C.

Polymer discs for the dynamic surface studies were photo-polymerized using the same UV chamber as above, with a PDMS mold of the titanium surfaces (PT, A, or GB) on the bottom glass slide, without glass spacers, and the top glass slide carefully slid over the top of the PDMS to create a seal. After post-cure, excess polymer was snapped off of discs and the edges lightly sanded prior to soaking in distilled water for 3 days at 37°C, to remove excess monomer, after which the discs were dried overnight. Discs were then sterilized by UV light (λ=254 nm) for 90 min.

### 3.2.2 Swelling characteristics

Percent weight change, volume change, and swelling ratio were determined at 1 and 7 days. Samples were measured and weighed prior to immersion in phosphate buffered saline (PBS; Sigma-Aldrich), at 1 day and 7 days after immersion, and after 24 hours of drying under vacuum. Water content was determined from change in weight % by $\%w = \frac{\text{weight}_{wet} - \text{weight}_{dry\,(vacuum)}}{\text{weight}_{dry}}$. Similarly, the volume change was

expressed by $\%v = \frac{\text{volume}_{\text{wet}} - \text{volume}_{\text{dry (vacuum)}}}{\text{volume}_{\text{dry}}}$. Finally, the swelling ratio was simply the wet weight normalized by the dry weight (n=3).

### 3.2.3 Thermomechanical testing

Dynamic mechanical analysis (DMA) in tensile loading was used to determine the Tg and rubbery modulus of the networks (TA Q800 DMA, Newcastle, DE). Rectangular samples (1 x 5 x 15 mm3) were laser cut from polymer sheets and their edges were sanded using grit paper. The samples were thermally equilibrated at -75°C for 2 min and then heated to 200°C at a rate of 5°C/min. Testing was performed in cyclic strain control at 0.2% strain with a preload force of 0.001 N and a force track setting of 150%. Tg was defined as the peak of the tan delta curve, and the rubbery modulus was taken 20°C beyond the lowest point in the rubbery plateau (n=3).

Differential scanning calorimetry (DSC) was also used to determine if submersion for 7 days would affect the Tg of the networks (TA Q100 DSC, Newcastle, DE). Samples were weighed (average mass between 10 and 14 mg) prior to testing. Samples were equilibrated at -80°C and subsequently heated to 200°C at a rate of 5°C/min. The Tg was denoted as a step change on the DSC curve, indicating a second order endothermic transition (n=3).

### 3.2.4 Surface characterization

Surface wettability was determined by performing contact angle measurements using the sessile drop method on a Ramé-hart Model 250 goniometer (Mountain Lakes, NJ). A 2 μL drop of deionized water was dropped onto the disc surface, and the contact angle between the side of the drop and the polymer surface was measured using a camera

and DROPimage software (Mountain Lakes, NJ). Five measurements per disc were taken on three discs of each roughness.

Elemental analysis was performed by X-ray photoelectron spectroscopy (XPS) on a Thermo K-alpha XPS (Thermo Scientific, Waltham, MA) under high vacuum (5 < 10-7 Torr) using Al Kα radiation with a pass energy of 200 eV for survey scans and 50 eV for elemental scans, a 400 μm spot size, and 50 ms dwell time. Peak assignments and their corresponding area were determined using Advantage Data System (Thermo Scientific). Survey scans were done in duplicate and elemental scans in triplicate on three spots per disc for two separate discs of each roughness.

Surface roughness for both titanium and polymer discs was evaluated by laser scanning microscopy (LSM) and profilometry. A Zeiss LSM 710 (Zeiss, Jena, Germany) at 20x magnification was used to scan areas of 500x500 $\mu m^2$ with a 100 μm cutoff wavelength to determine average surface area roughness (Sa) and height (Sz). Three scans per disc were performed on three separate discs of each roughness and material type.

Surface morphology was examined by scanning electron microscopy (SEM). Polymer discs of each roughness were coated with a thin layer of gold with a Technics Hummer V Gold Sputterer and imaged using a Hitachi S-4700 FE-SEM (Hitachi High Technologies America, Gaithersburg, MD). Ti disc scans were performed at 10 kV and coated polymer discs at 5 kV.

### 3.2.5 Compression

SMP-programmed polymer discs with smooth surface topographical features were created via compression on an MTS Insight equipped with a 2 kN load cell, Testworks 4 programming system and a thermal chamber to control the environmental temperature. The

sample was loaded onto an aluminum constraint device of 15 mm in diameter on top of a compression platen inside the thermal chamber, and the top compression platen was lowered until just touching the top of the disc. To minimize artifacts induced from the platen surface, smoothed aluminum foil was placed over the top platen. The sample was then heated to a temperature of 90°C and allowed to equilibrate for 15 minutes prior to compression. The top platen was lowered at a speed of 1 mm/min until 35% strain was reached, as determined by the crosshead position. Data was acquired at 10 Hz. Samples were sputter coated with gold and imaged with a JEOL LV-5610 SEM (JEOL Ltd., Tokyo, Japan) before and after compression at 5 kV (n=2).

### 3.2.6 Surface recovery

The free strain recovery of the programmed polymer surfaces was evaluated by placing the polymer discs in PBS at 37°C. Samples were removed at 1h, 2h, 3h, 4h, 12h, 24h, and 48h to have their roughness measured using LSM. A Zeiss LSM 710 with settings as described above was used to determine Sa. Three scans were performed per disc on three separate discs at each time point.

### 3.2.7 Cell culture

Human MG63 osteoblast-like cells (ATCC, Manassas, VA) were cultured in Dulbecco's modification of Eagle's medium (DMEM, Cellgro, Manassas, VA), 10% fetal bovine serum (Hyclone, Waltham, MA), and 1% penicillin-streptomycin (Invitrogen, Carlsbad, CA) at 37°C, 5% CO2, and 100% humidity. To overcome the buoyancy of the polymer discs, CellCrown polymer inserts (Scaffdex, Finland) were used to keep the discs at the bottom of the cell culture wells. Depending upon the experiment, cells were plated onto one of several surfaces: tissue culture polystyrene (TCPS), titanium discs (Ti PT, Ti

A, Ti GB), static polymer discs with three different topographies (pPT, pA, pGB), or dynamic polymer discs with programmed recovery of the grit-blasted surface (dyn pGB). Cells were plated at a density of 20,000 cells/cm2 and cultured for 24 hours. Media were changed at that time. For some experiments, cells were either harvested or were cultured for an additional 48 hours. Each variable was tested in 6 independent cultures in each experiment.

### 3.2.8 Static disc cellular response analysis

To assess any effects of the polymer on cell viability, MG63 cells were cultured on TCPS and smooth co-polymer discs, varying the crosslinker content. At 1 day and 7 days post-plating, cell viability was determined by measuring the reduction of resazurin using the Alamar Blue assay (AbD Serotec, Raleigh, NC) and by measuring cell metabolic activity using the MTT assay (Sigma-Aldrich). To assay effects of the polymer on cell response, conditioned media were collected 24 hours post-confluence on TCPS and osteocalcin levels measured by radioimmunoassay (Biomedical Technologies Inc., Stoughton, MA). Levels of osteoprotegerin (R&D Systems) and vascular endothelial growth factor (VEGF) (R&D Systems) in the conditioned media were measured by ELISA according to the manufacturer's instructions, as described previously [1,2]. Cell layers were lysed and DNA, alkaline phosphatase specific activity, and protein levels were measured in the lysate (n=6). Alkaline phosphatase specific activity was normalized to total protein content of the cell layer lysates (BCA Protein Assay, Thermo Fisher, Pittsburgh, PA), and levels of secreted factors in the conditioned media were normalized to DNA content (Quant-iT™ PicoGreen dsDNA Assay, Life Technologies, Carlsbad, CA).

### 3.2.9 Cell morphology

To examine the effect of dynamic surface roughness, MG63 cells were cultured on compressed SMP surfaces, and on smooth and rough static surfaces without compression as control, and cell morphology was examined by SEM and LSM. For SEM, cells were plated as described and cultured for 3 h, 6 h, 12 h, 24 h, and 48 h. At each time point, the media were removed, and the samples were rinsed three times with PBS to remove excess media. Samples were fixed with Karnovsky's fixative (Electron Microscopy Sciences, Hatfield, PA) for 24 h at room temperature. After fixation samples were freeze-dried for 48 h. Samples were sputter coated with gold (Hummer V Gold Sputterer, Technics) and imaged using either a Hitachi S-4700 FE-SEM with an SE2 detector (Hitachi High Technologies, Schaumburg, IL) or JEOL LV-5610 SEM (JEOL Ltd., Tokyo, Japan) (n=2). For LSM, MG63 cells were plated as described and cultured for 2h, 4h, 6h, 8h, 12h, and 24h. At each time point, the media were removed and the samples rinsed twice with warmed PBS. Samples were fixed with Karnovsky's fixative overnight at 4 °C, washed three times with PBS, permeabilized with 0.1% Triton X-100 for 15 min, washed again with PBS, and incubated for 20 minutes in the dark with Hoescht for nuclear staining (Life Technologies, 1:1000) and phalloidin for f-actin staining (Alexa Fluor 633, 1:50, Life Technologies). Images were taken on a Zeiss LSM 710 microscope at 20x magnification (n=2).

**3.2.10 Dynamic disc cellular response analysis**

At 1 day and 3 days post-plating, conditioned media were collected and levels of osteocalcin (Biomedical Technologies Inc.), osteoprotegerin, VEGF, and FGF2 in the conditioned media were measured by ELISA as described previously [23, 24]. MG63 cell layers were lysed and DNA, alkaline phosphatase specific activity, and protein levels

were measured in the lysate as described above. In addition, to assess whether the effects of the SMP substrates were maintained over time, we examined cultures at 7 and 10 days post-plating.

### 3.2.11 Statistical analysis

Mean +/- standard deviation was calculated for all measurements described in Sections 3.2.2, 3.2.3, 3.2.4 and 3.2.6. Experiments described in Section 3.2.7 and 3.2.8 were performed at a minimum in duplicate and data shown are from a representative experiment. For cellular studies, values given are the mean ± SEM of six individual cultures per variable. Experiments were repeated at least five times in order to validate observations with the exception of supplemental experiments. Treatment over control ratios were determined for these studies. Results examining longer term behavior of cells cultured for 7 and 10 days are from one of two experiments, each experiment having an N=6 independent cultures per variable. In all cases, data were analyzed via analysis of variance (ANOVA) and when differences were detected, by post hoc analysis using Bonferonni's modification of Student's t-test. Significance was determined as $p < 0.05$.

## 3.3 Results

### 3.3.1 Material Characterization

In order to achieve polymer networks with the appropriate moduli and shape recovery behavior under in vitro conditions, we first characterized the effect of crosslinker concentration on water content and thermomechanical properties (Fig 3.2A). There was negligible percent weight or volume change after seven days in PBS for all groups except the 1% crosslinker, which had approximately 2% volume change. These

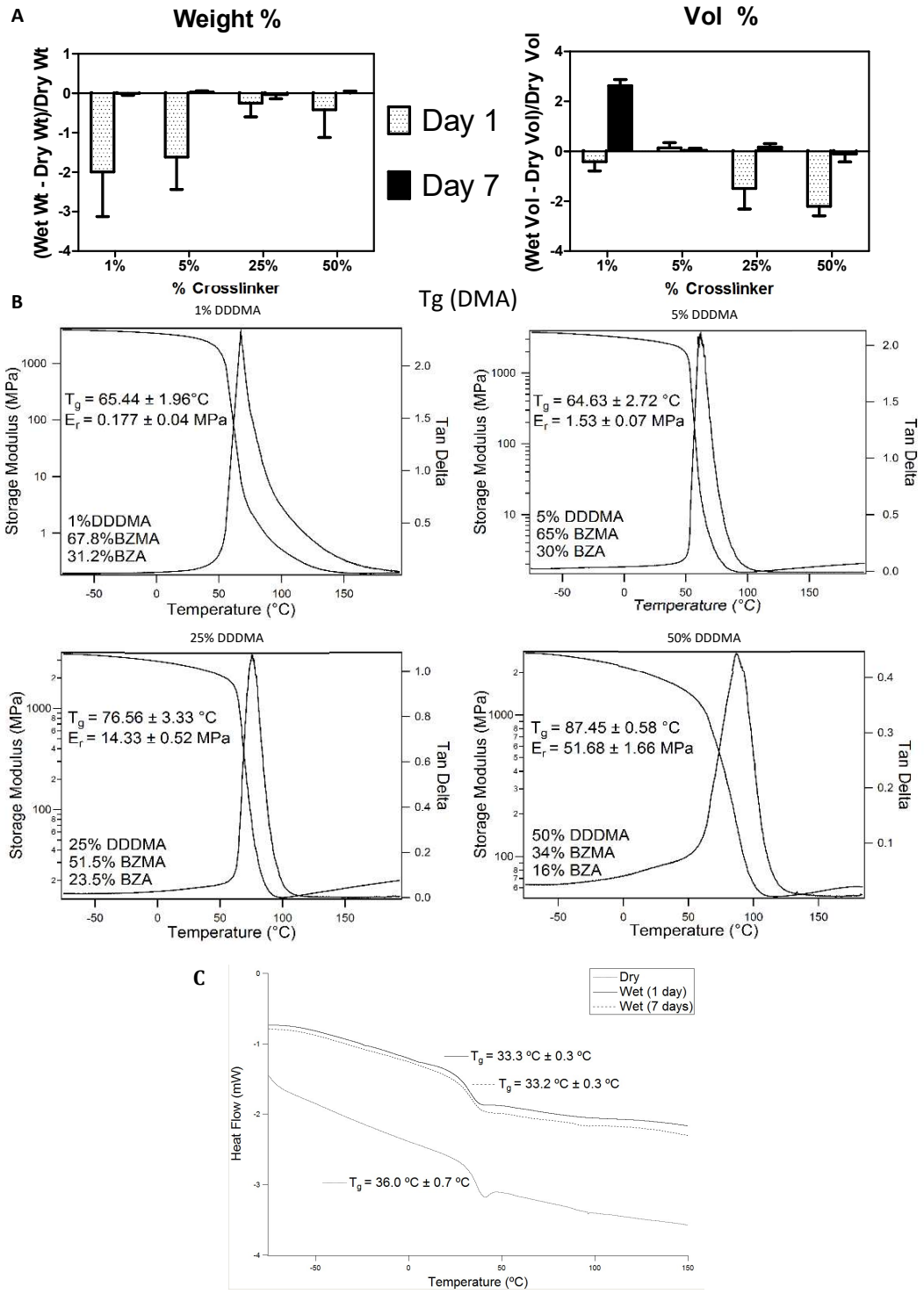


**Figure 3.2** Characterization of networks. A) Weight percent and volume percent of 1-50% DDDMA crosslinked networks. B) Dynamic mechanical analysis of 1-50% DDDMA crosslinked networks (peaks are tan-δ, curves representative). C) Differential scanning calorimetry to determine Tg of both dry and wet (1 day and 7 days) 30:65:5 BZMA:BZMA:DDDMA networks.

results indicated that the networks did not swell when placed in an aqueous environment.

Increasing crosslinker concentration did not affect Tg until 25% weight content at which point it began to act as a primary component to increase the Tg (Fig. 3.2B). In contrast, the differences in Er were apparent even between 1% and 5%, increasing the modulus tenfold. For the remaining materials characterization and experiments, a 5% crosslinking concentration (30% BZA, 65% BZMA, 5% DDDMA) was chosen as this concentration allowed the copolymer to have the appropriate modulus and failure strain needed to successfully undergo the shape memory cycle [6]. DSC showed a slight decrease in Tg after soaking for 1 day but no change after that up to 7 days for wet samples (Fig. 3.2C).

Like GB Ti, pGB samples showed a significant increase in roughness and peak-to-valley height over pPT and pA (Fig. 3.3A). There was no significant difference in

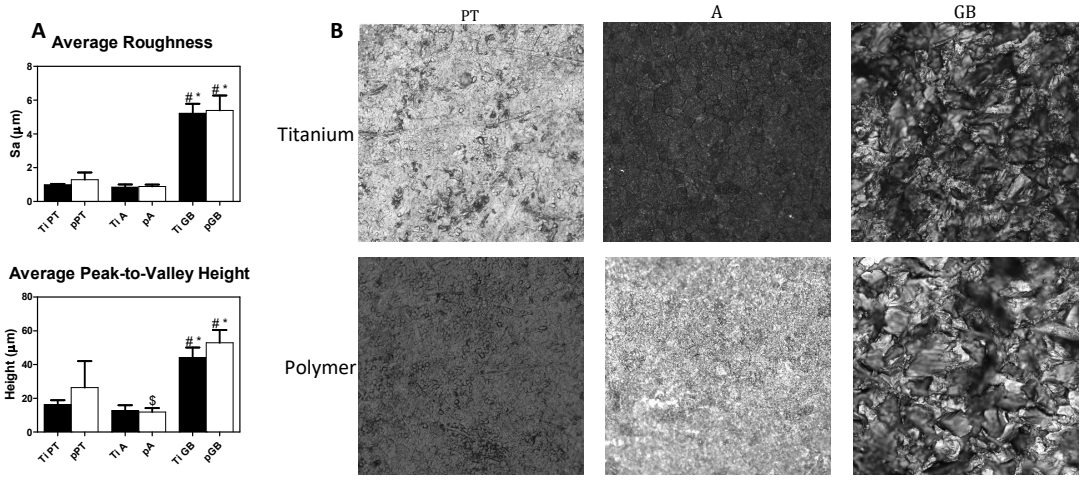


C

| Sample | XPS Concentration (mean at.% ± SD) | | | Contact Angle [° ± SD] |
|---|---|---|---|---|
| | C | O | Si | |
| pPT | 71.9 ± 0.8 | 20.8 ± 0.2 | 7.1 ± 0.5 | 93 ± 2 |
| pA | 70.4 ± 0.5 | 20.7 ± 0.2 | 8.2 ± 0.1 | 100 ± 2 |
| pGB | 67.7 ± 2.3 | 21.7 ± 0.7 | 9.7 ± 1.3 | 94 ± 4 |

**Fig. 3.3** Characterization of shape-memory polymer networks. **A**) Average roughness and peak-to-valley height for titanium discs of varied roughness and corresponding 30:65:5 BZA:BZMA:DDDMA discs. $p<0.05$ *=vs all PT; #=vs all A; $=vs pPT. **B**) Confocal images of titanium discs and corresponding 30:65:5 BZMA:BZA:DDDMA discs. Scale bar = 100 µm. **C**) Concentration of surface elements and corresponding contact angle on 30:65:5 BZA:BZMA:DDDMA discs of varied roughness.

roughness between the Ti PT and pPT surfaces, Ti A and pA surfaces, nor Ti GB and pGB surfaces, indicating successful transfer of topography onto the polymer. This was confirmed by confocal (Fig. 3.3B) and SEM imaging (Fig. 3.4). XPS analysis showed that the polymer surfaces had equivalent carbon and oxygen concentrations with some contamination of silicon from processing (Fig. 3.3C). The polymer surfaces had similar contact angles of 93-100 degrees.

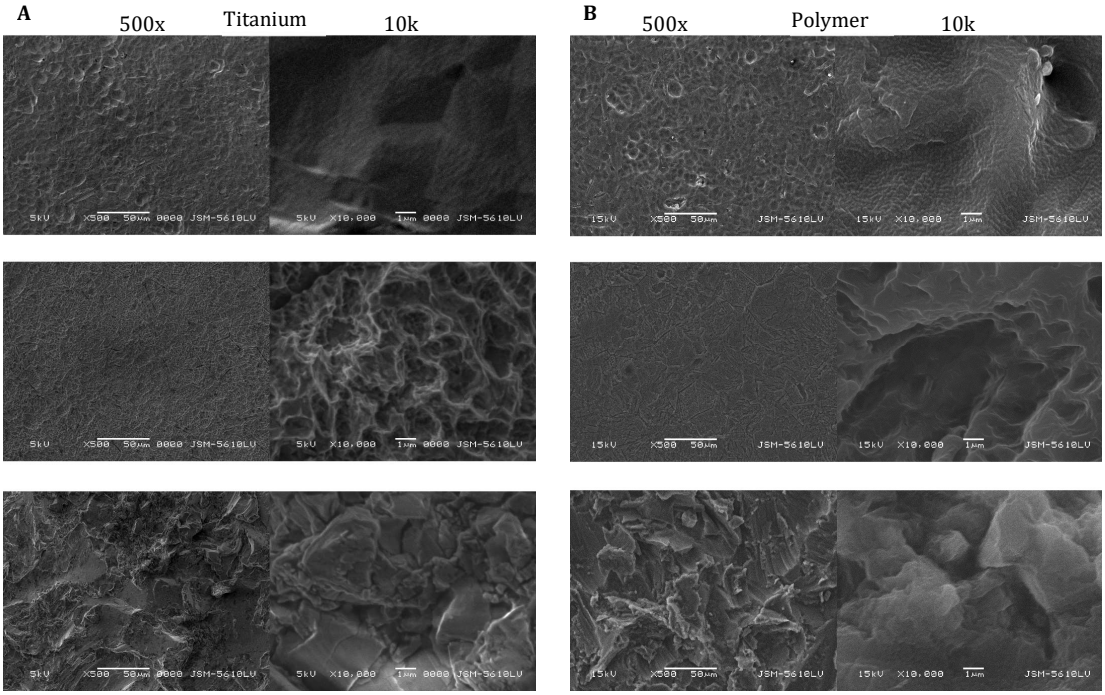


**Figure 3.4** SEM images of titanium (A) and polymer (B) discs. Scale bar = 50 μm for 500x images, 1 μm for 10kx images.

**Cellular response to static surfaces**

Overall, growth of MG63 cells on smooth co-polymer surfaces was similar to growth on TCPS (Fig. 3.5A). At one day post-plating, there was less metabolic activity in wells with polymer surfaces compared to TCPS, but by day 3, cultures on all surfaces had comparable AlamarBlue staining and at day 7, only cultures growth on copolymer made with 50% crosslinker had reduced metabolic activity based on this assay. In contrast to

AlamarBlue, MTT analysis indicated reduced cell viability on all polymer surfaces compared to TCPS at day 3. However, by day 7, there was a dose-dependent increase in MTT on the polymer surfaces: MTT on 1% crosslinker was less than on TCPS; activity on 5% crosslinker was comparable to TCPS; on 25% crosslinker it was greater than TCPS; and MTT on 50% crosslinker was higher than on 25%.

When cultures were grown on polymers with 5% crosslinker, surface roughness did not affect DNA content (Fig. 3.5B), alkaline phosphatase specific activity (Fig. 3.5C), or production of OPG (Fig. 3.5D) and VEGF (Fig. 3.5E). However, there was a significant

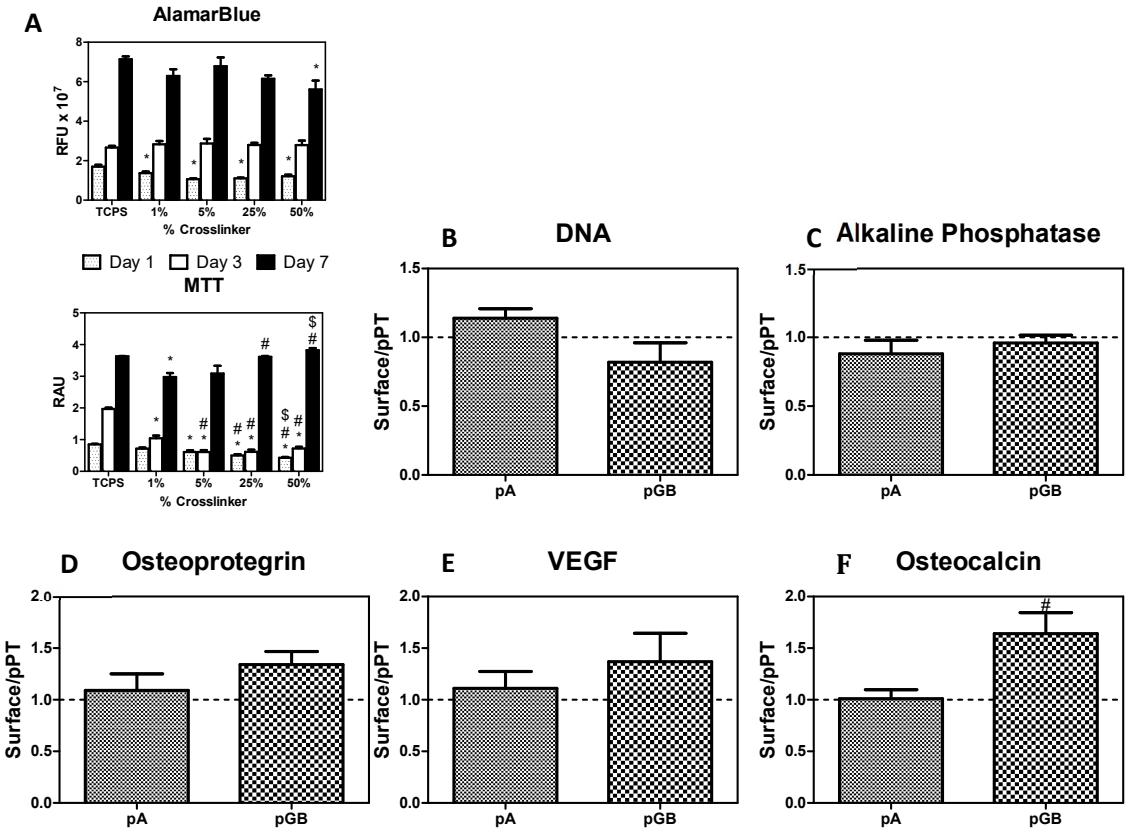


**Figure 3.5** MG63 behavior on static 30:65:5 networks. **A**) Cell viability assays confirming non-cytotoxicity of 1-50% DDDMA crosslinked networks. **B**) DNA quantification. **C**) Alkaline phosphatase specific activity. **D**) Level of secreted protein osteoprotegrin. **E**) Level of secreted protein VEGF. **F**) Level of secreted protein osteocalcin. $p<0.05$ #=vs pA (Average of 5 experiments)

increase in osteocalcin in cultures grown on pGB compared to cells cultured on both pPT and pA surfaces (Fig. 3.5F).

### 3.3.2 Shape memory characteristics

Confocal microscopy revealed that the roughness of the shape memory programmed polymer networks of pGB decreased by 80% compared to their initial roughness pre-compression (Fig. 3.6A). Percent original roughness was calculated as

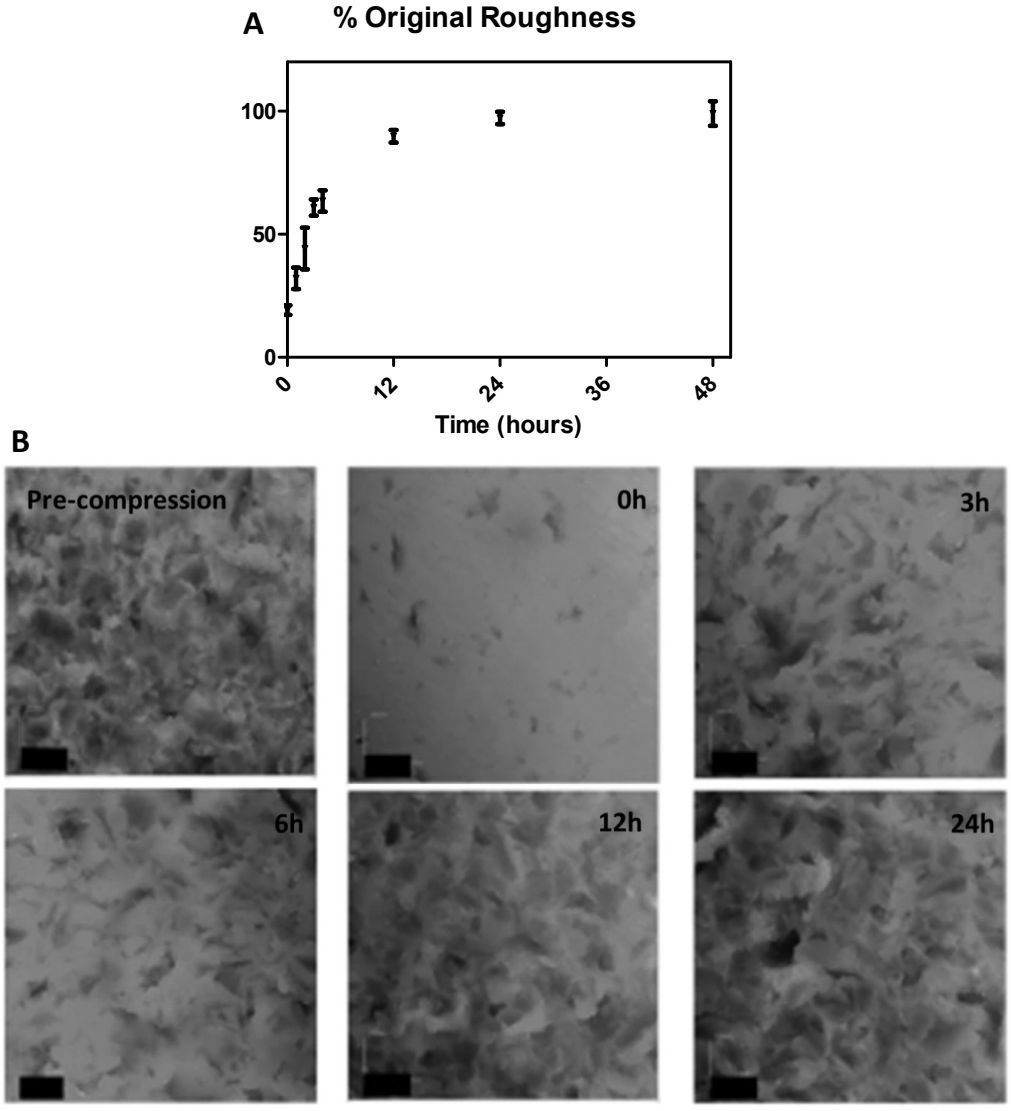


**Figure 3.6** Recovery of roughness on shape-changing 30:65:5 polymer networks. **A**) Recovery of original roughness. **B**) Confocal images of pre- and post-compression dynamic 30:65:5 networks recovering at 37 °C in PBS. Scale bar = 100 μm.

(measured roughness/original roughness)*100. Upon placement of the programmed pGB discs in PBS at 37°C, the samples exhibited 100% recovery within 24 hours with the majority of recovery occurring within the first 8 hours. Compression effectively removed peaks and filled most valleys, as seen by LSM images taken prior to compression (Fig. 3.6B, "Pre-compression") and after compression before recovery (Fig. 3.6B, "0h"). After

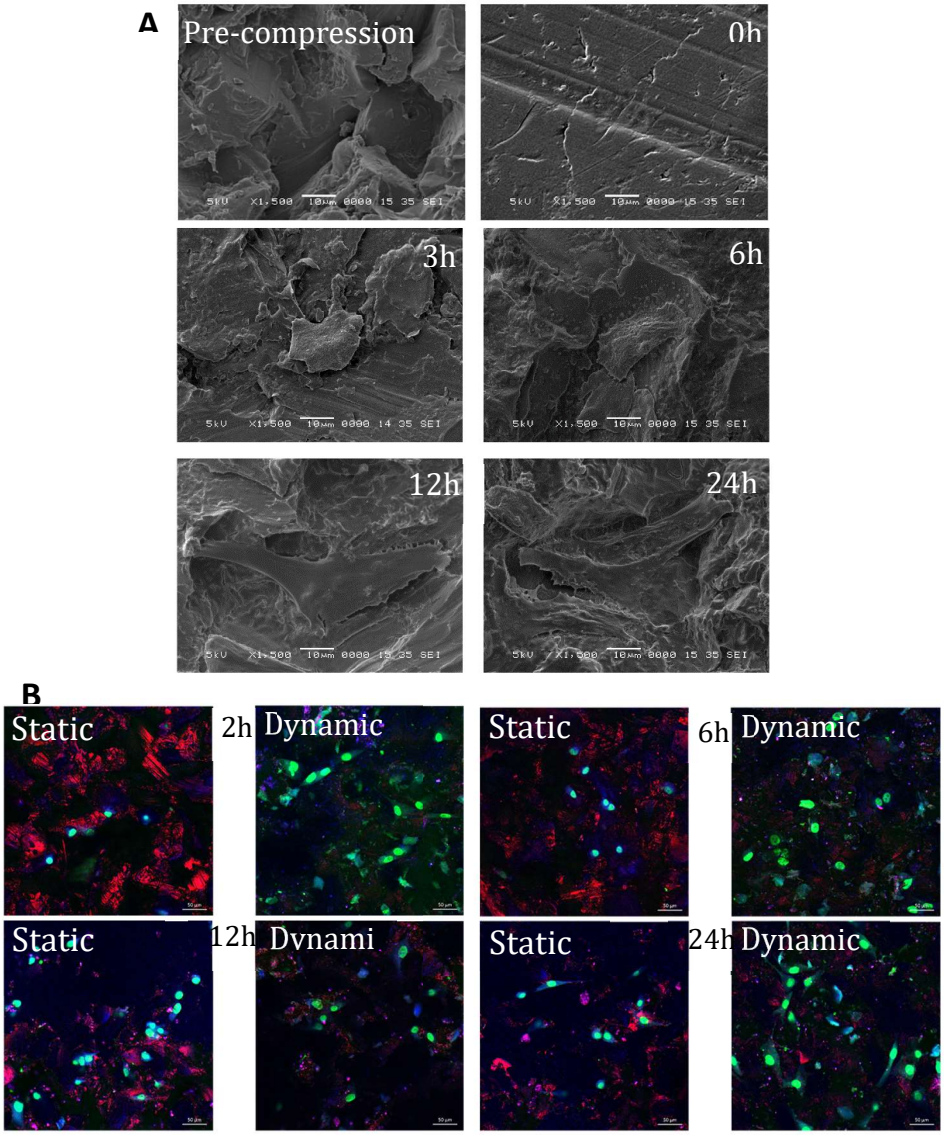


**Figure 3.7** Cell morphology on 30:65:5 polymer networks. **A**) SEM images of pre- and post-compression (0h) and MG63 cell morphology on dynamic 30:65:5 networks. Scale bar = 10 μm. **B**) Confocal images of MG63 cells on static and dynamic networks. Nuclei are stained with Hoescht (green) and actin with phalloidin (blue). Red is autofluorescence. Scale bar = 50 μm.

3 hours in PBS at 37°C, some recovery was evident on the surface (Fig. 3.6B, "3h") which increased after 6 hours and 12 hours (Fig. 3.6B, "6h", "12h" respectively). By 24 hours full recovery had occurred (Fig. 3.6B, "24h").

### 3.3.3 Cellular response to dynamic surfaces

No differences in MG63 cell morphology were observed in SEM images of dynamic pGB surfaces at t=0 (Fig. 3.7A, "Pre-compression", "0h"). Cells remained well spread out within 12h (Fig. 3.7A, "3h", "6h", "12h") over the first 24 hours post plating (Fig. 3.7A). LSM on both static and dynamic SMPs at 2, 6, 12, and 24 hours post-plating showed that morphology of cell nuclei and actin filaments was unchanged (Fig. 3.7B). For the initial 8 hours, more cells were observed on the dynamic surfaces than on static ones (data not shown).

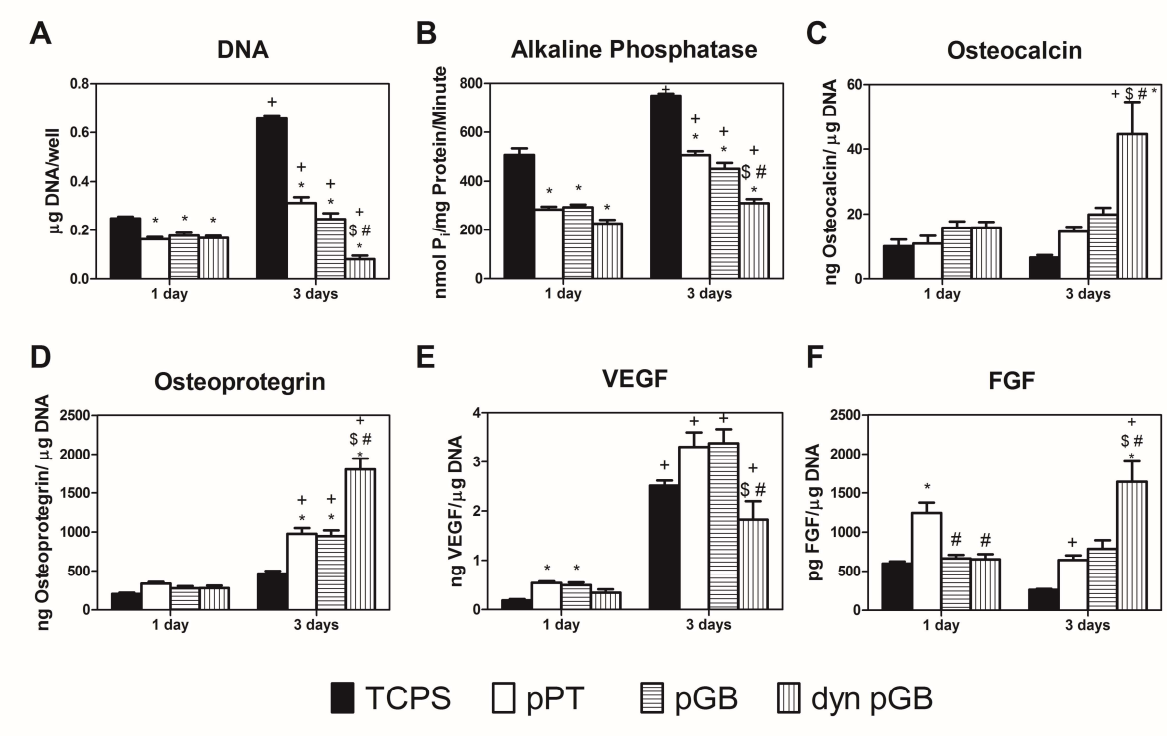


**Figure 3.8** MG63 behavior on 30:65:5 networks (1 day and 3 day). **A**) DNA quantification. **B**) Alkaline phosphatase specific activity. **C**) Level of secreted osteocalcin. **D**) Level of secreted osteoprotegerin. **E**) Level of secreted VEGF. **F**) Level of secreted FGF2. $p<0.05$ *=vs TCPS; #=vs pPT; $=vs pGB; +=vs 1 day.

Attachment of MG63 cells was reduced on static and dynamic polymer substrates compared to TCPS, but was not affected by surface topography. At 1 day post plating, there was significantly less DNA in cells grown on static pGB, static pPT, and dynamic pGB surfaces compared with TCPS with no differences to each other (Fig. 3.8A). DNA content in MG63 cells on static surfaces increased on day 3 compared to day 1, but the amount of DNA on the dynamic surface (dyn pGB) decreased, and cells grown on all polymer surfaces had lower DNA content than those grown on TCPS.

Alkaline phosphatase specific activity was reduced on the polymer disks compared to TCPS but was comparable across all polymer groups at 1 day (Fig. 3.8B). Activity increased in cultures grown on all substrates at 3 days. This increase was greatest on TCPS compared to pPT and pGB. Cells grown for 3 days on dyn pGB saw the lowest increase in enzyme activity. Osteocalcin levels in the conditioned media at day 1 was comparable in all groups (Fig. 3.8C). Only cells on dyn pGB group exhibited an increase in osteocalcin at 3 days. Production of osteoprotegrin was comparable in all cultures at day 1 (Fig. 3.8D). At day 3, cells on dyn pGB exhibited the greatest increase in osteoprotegerin in their conditioned media; cells on static pPT and pGB also exhibited increased osteoprotegerin compared to TCPS, but levels were less than on dyn pGB. MG63 cells grown on the static pPT and pGB surfaces produced more VEGF at 1 day than cells on TCPS or dyn pGB (Fig. 3.8E). All groups had increased VEGF on day 3, with the highest amounts seen from cells cultured on the static pPT and pGB surfaces (Fig. 3.8E). The dyn pGB group had statistically lower amounts of VEGF compared to the static surface groups but was not statistically different than the group cultured on TCPS. Another angiogenic growth factor, FGF2, was greatest in static pPT cultures on

day 1. At 3 days the static pPT group had decreased but FGF2 continued to increase in cultures grown on dyn pGB surfaces (Fig. 3.8F).

To confirm the effect of the dynamic shape memory recovery, we repeated the previous experiment five times and evaluated the results by normalizing the static pGB and dyn pGB groups to the static pPT group. At 3 days post-plating the cells that were cultured on the dyn pGB surfaces had statistically less DNA than those grown on all static surfaces (Fig. 3.9A), and while cells cultured on both static and dynamic surfaces had similar amounts of alkaline phosphatase specific activity (Fig. 3.9B), cells grown on dyn pGB surfaces had twice as much osteocalcin levels (Fig. 3.9C) and one and a half times as much osteoprotegerin (Fig. 3.9D). There were no statistical differences in the levels of VEGF and FGF2 between the cell groups cultured on the static and dynamic surfaces (Fig. 3.9E-F).

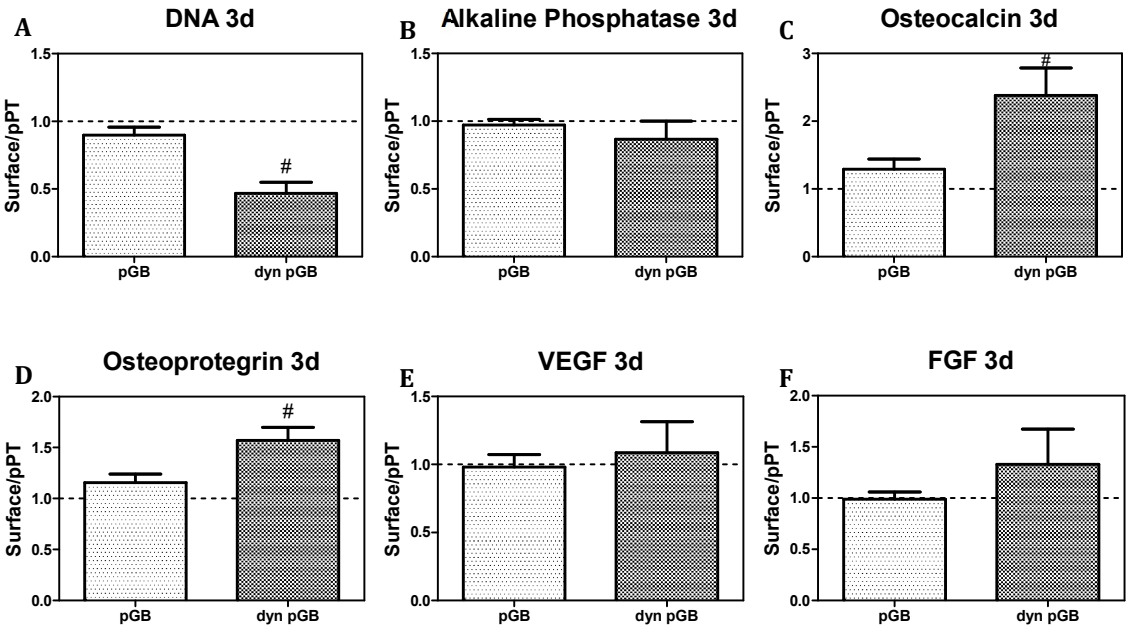


**Fig. 3.9** MG63 cell behavior on 30:65:5 networks (static and dynamic). **A**) DNA quantification. **B**) Alkaline phosphatase specific activity. **C**) Level of secreted osteocalcin. **D**) Level of secreted osteoprotegerin. **E**) Level of secreted VEGF. **F**) Level of secreted FGF2. $p<0.05$ #=vs pGB (Average of 5 experiments).

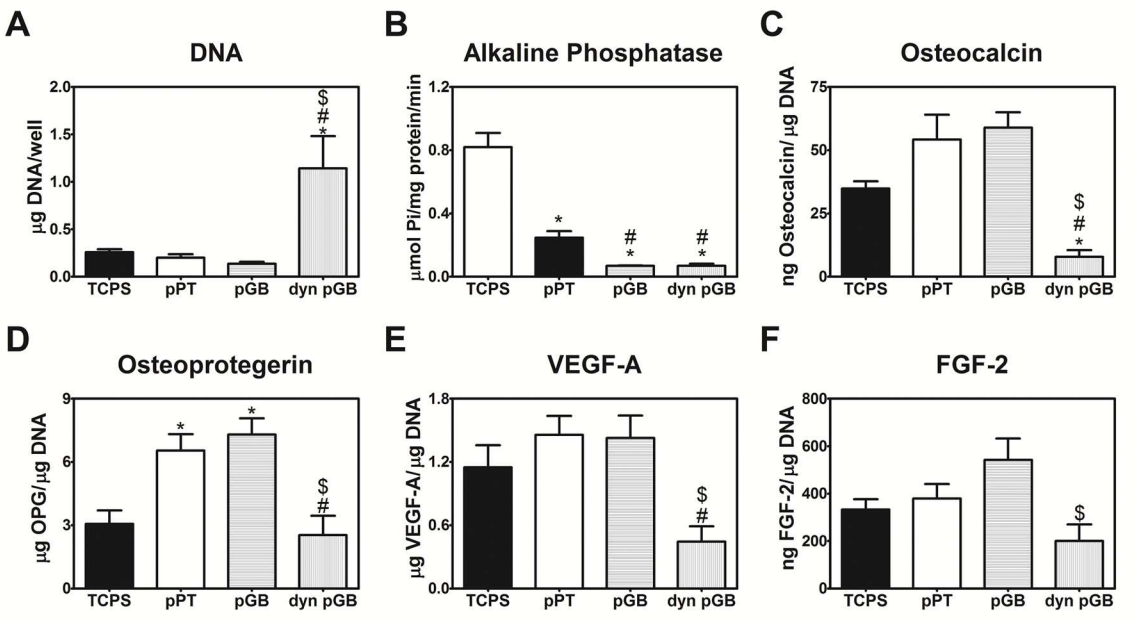


**Figure 3.10** MG63 cell behavior on 30:65:5 networks (7 day). **A**) DNA quantification. **B**) Alkaline phosphatase specific activity. **C**) Level of secreted osteocalcin. **D**) Level of secreted osteoprotegerin. **E**) Level of secreted VEGF. **F**) Level of secreted FGF2. $p<0.05$ *=vs TCPS; #=vs pPT; $=vs pGB.

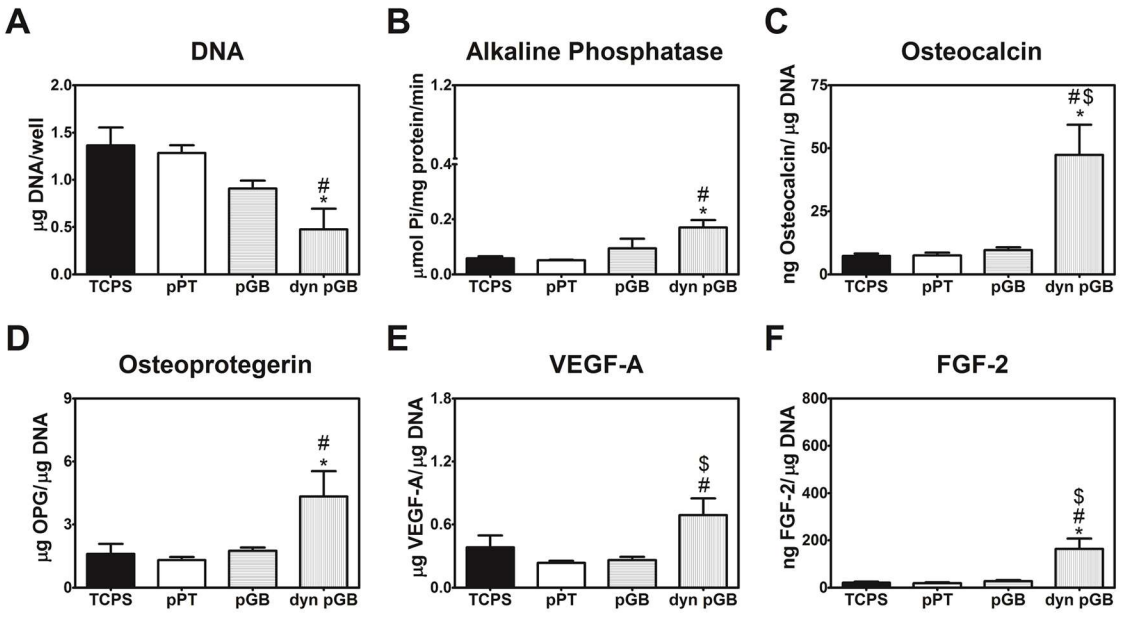


**Figure 3.11** MG63 cell behavior on 30:65:5 networks (10 day). **A**) DNA quantification. **B**) Alkaline phosphatase specific activity. **C**) Level of secreted osteocalcin. **D**) Level of secreted osteoprotegerin. **E**) Level of secreted VEGF. **F**) Level of secreted FGF2. $p<0.05$ *=vs TCPS; #=vs pPT; $=vs pGB.

At longer time points (7 days), the dyn pGB group exhibited an increase in DNA (Fig.

3.10) but was statistically lower than the other groups at day 10 (Fig. 3.11), and at day 10 the dyn pGB group had statistically higher levels of osteocalcin, osteoprotegrin, VEGF, and FGF (Fig. 3.11).

## 3.4 Discussion

Numerous in vitro studies from our lab and others have shown that microrough Ti and Ti alloy surfaces promote osteoblastic differentiation of cells in the osteoblast lineage at the expense of attachment and proliferation. Our results using a shape memory polymer system suggest that this limitation can be addressed using smart materials that provide an initial smooth surface to enable cell attachment and proliferation, but shift to a microtextured topography to stimulate osteoblast differentiation. We show that polymer surfaces can be generated that mimic microtextured surfaces on Ti and Ti alloys. Under static conditions cell growth on the polymers is comparable to growth on TCPS, even when microtextured substrates are used. However, production of osteocalcin is higher on microtextured polymer surfaces, indicating that differentiation is enhanced. The effects of surface microtopography are even more striking in cultures grown under dynamic conditions. Moreover, they are time-dependent. DNA content and alkaline phosphatase activity are reduced compared to static microrough cultures, but differentiation is stimulated based on marked increases in production of osteocalcin and osteoprotegerin. Taken together, our results suggest that smart materials can be developed that optimize time-dependent proliferation and differentiation of osteoprogenitor cells based on physical cues.

To date, there have been few studies that examine the shape memory effect of polymer surfaces on the in vitro cellular response [60-66], and specifically, none that report how the shape recovery of surface topography affects osteoblast differentiation. In this

study, we fabricated and characterized a novel, nontoxic acrylate copolymer material that can be programmed to gradually increase in roughness upon exposure to in vitro conditions. This dynamic recovery enhances the production of osteogenic growth factors including osteocalcin and osteoprotegerin in as little as three days and greatly increases these factors at ten days. Our data also may suggest that in long term cultures, growth and differentiation of MG63 cells on the microtextured dynamic SMP substrates occurs in alternating cycles of proliferation and osteoblastic phenotypic expression.

The composition of the copolymer was tailored such that its activation temperature was just above body temperature allowing for partial recovery of the surface features upon heating to 37°C. Monomers with hydrophobic chemistries were selected to reduce any swelling effects that might alter the surface topography. The overall hydrophobicity also allowed for a small gradual uptake in water. The few degrees decrease in the activation temperature (Tg) upon immersion in water matches the behavior of other polymer networks with similar hydrophobicity reported in previous studies [37]. The same micro-scale surface features as those on titanium were able to be successfully transferred onto the copolymer via soft lithography techniques. By compressing the surface above Tg, this topography could be eliminated and then 100% recovered upon heating to body temperature in solution. We chose grit-blasted roughness (pGB) for use in our dynamic studies because while it had the same chemistry as the pPT and pA discs, it produced a more noticeable effect on osteocalcin levels but did not have an effect on proliferation or other growth factors. This suggests that an acrylate copolymer's surface topography, specifically the grit-blasted surface features, can influence the osteogenic response, as has been shown on titanium [31,32,46,47,67].

Once the MG63 cells were exposed to the dynamic topography, the shape recovery not only enhanced osteocalcin production compared to the static rough surfaces but also had an effect on the other growth factors. This change from smooth to rough over a relatively short time had an effect on osteocalcin, osteoprotegrin, and differentiation (shown by the decrease in cell number) at 3 days. The results at 10 days suggest this effect could be even more pronounced but needs to be confirmed with further studies. Alternatively, to have a material that undergoes shape recovery over 48 hours could lead to much better effects for osteoclasts, or an 'optimal' time frame of shape recovery with different cell types could result in a family of new products for various tissue regeneration applications.

The results indicate that there are two stages to the osteoblast response to the dynamic surface topography. During the first stage, there is no effect from the surface recovery of roughness on MG63 cell DNA or other factors, but in the second stage there is an effect attributed to surface recovery of roughness. The time during which cells were adhering and just beginning to proliferate was simultaneous with the recovery of the rough surface features – that is, roughly 8 hours. This explains why at 1 day we see no differences in the amount of cell DNA on the polymer surfaces, but at 3 days on the dynamic surfaces we have enhanced differentiation and growth factor production; by this time, cells had been growing on the already changed surfaces for 24 hours.

Previous studies have suggested that acrylate copolymer networks cannot elicit a strong osteogenic response compared with titanium due to the effects of the surface chemistry [37]. The results of this present study demonstrate that MG63 cells exposed to a dynamic surface from smooth to rough on an acrylate-based copolymer network produce

a similar favorable osteogenic response typically observed on titanium, indicating that a temporal change in topography can override any effect due to polymer chemistry (preliminary data, not shown). One explanation for this is that the MG63 cells are undergoing a mechanical conditioning during the smooth state (in the first stage) to respond more during the rough state (in the second stage). Under this premise, an SMP with a delayed onset of recovery or a longer recovery time (for example over two or three days) would allow for more proliferation before inducing rapid differentiation. It remains to be seen whether the speed of recovery of the surface topography has an impact on the degree of biological response. The effect of the recovery rate could potentially be investigated in future studies by changing the copolymer composition and programming conditions. Previous published work with non-degradable SMPs has been limited to examination of cell alignment on surfaces that change from aligned or grooved to random[61] or smooth[62]. This is the first study looking at smooth-to-rough transition with topography known to induce osteoblast differentiation[47].

Our use of soft lithography combined with SMP surface programming could be applied to other scaffolds where it would be beneficial to transition between different surface structures over time. For example, aligned SMP scaffolds for neural or myogenic direction cell growth, or biodegradable SMP scaffolds which change on the same time scale as immune responses. Future in vivo studies could confirm clinical applications of this method.

# CHAPTER 4

# EFFECTS OF STIFFNESS AND ROUGHNESS ON OSTEOBLAST DIFFERENTIATION

## 4.1 Introduction

The microenvironment of a cell says much to direct it, sometimes even more so than the chemical clues given to it [68]. Though the specific mechanisms behind how a cell senses roughness or microtopography are largely unknown (compared to something such as stiffness), some work has been done in this area [69-72]. One study examining the adhesive behavior of cells when presented with varied RGD density due to differences in roughness and stiffness concluded that fibroblast cell attachment depended largely on the spacing of the ligand (roughness) and secondly on the stiffness of the substrate [73]. Others have claimed that for stem cells, stiffness has the greater role in directing differentiation [74]. Much remains unknown with respect to specifics or whether mechanisms to sense stiffness are shared to sense roughness.

The objective of this study was to determine if stiffness *and* roughness has an effect on MG63 differentiation into osteoblasts. To address this question, we first had to create materials of differing stiffness and roughness. We chose methyl acrylate (MA) methyl methacrylate (MMA) poly(ethylene glycol) dimethacrylate (PEGDMA) polymers due to evidence showing clear, distinct human osteoblast response (see APPENDIX A, [37]) and PT and GB roughness which on a different acrylate also showed responsiveness (see previous chapter).

## 4.2 Materials and Methods

### 4.2.1 Material fabrication and synthesis of samples

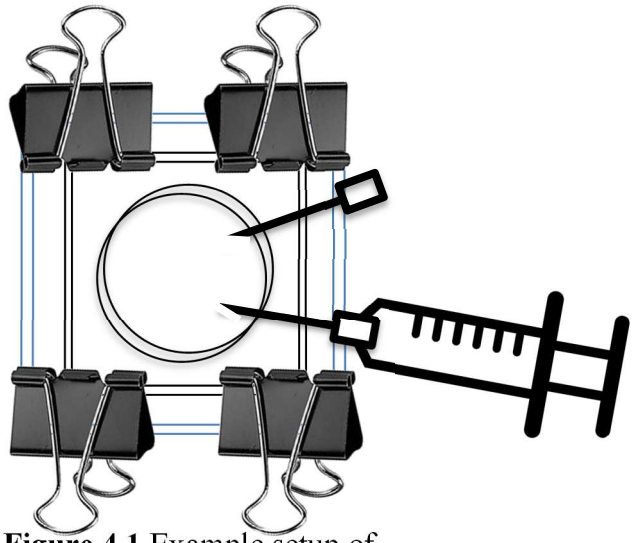

**Figure 4.1** Example setup of MA:MMA:PEGDMA solution injection into mold.

Methyl methacrylate (MMA), methyl acrylate (MA), and poly(ethylene glycol) dimethacrylate (PEGDMA MW~750) were obtained from Sigma-Aldrich (St. Louis, MO) and used as received. PDMS molds from PT and GB discs as described in 3.2.1 were cut into individual rectangles, placed between cleaned glass slides, and clamped at four corners using mini binder clips. The weight ratio of MA to MMA was varied while the crosslinking concentration of PEGDMA was held constant at 10 wt% to produce four copolymer networks (by wt. % of MA): 18MA, 29MA, 40MA, and 72MA. 0.5 wt.% 2,2-dimethoxy-2-phenylacetophenone (DMPA) was used as the photoinitiator (Sigma-Aldrich). A 27-gauge needle was placed into well to allow air to eject. Solutions were injected into a single well (see Figure 4.1). The excess needle was removed after the well was filled. Approximately one to two minutes later wells were filled again as needed and then photopolymerized in a UV chamber (Spectrolinker XL-1500, Spectroline, Westbury NY; $\lambda$ = 385nm) for 45 minutes. Discs in molds were then placed in an oven at 90˚C for 90 minutes to post-cure and the mold removed once at room temperature. Discs for cell studies were sterilized by UV light ($\lambda$=254 nm) for 90 min, washed with sterile Dulbecco's phosphate buffered saline (DPBS, Sigma-Aldrich), and incubated with medium used for cell culture (see section 4.2.3) for 5 minutes prior to plating.

### 4.2.2. Surface characterization

Surface roughness was evaluated by laser scanning microscopy (LSM). A Zeiss LSM 710 (Zeiss, Jena, Germany) at 20x magnification was used to scan areas of 500x500 $\mu m^2$ with a 100 μm cutoff wavelength to determine average surface area roughness (Sa) and height (Sz). Six scans per disc were performed on two separate discs of each roughness and stiffness. The polymer discs were then sputter coated with gold and imaged with a JEOL LV-5610 SEM (JEOL Ltd., Tokyo, Japan). Ti disc scans were performed at 15 kV and coated polymer discs at 5 kV.

### 4.2.3 Cell culture

Human MG63 osteoblast-like cells (ATCC, Manassas, VA) were cultured in Dulbecco's modification of Eagle's medium (DMEM, Cellgro, Manassas, VA), 10% fetal bovine serum (Hyclone, Waltham, MA), and 1% penicillin-streptomycin (Invitrogen, Carlsbad, CA) at 37°C, 5% CO2, and 100% humidity. To overcome the buoyancy of the polymer discs, CellCrown polymer inserts (Scaffdex, Finland) were used to keep the discs at the bottom of the cell culture wells. Cells were plated at a density of 20,000 cells/$cm^2$ for 24 hours at which point media was changed, and media changed every other day until 90% confluent on TCPS. At that point cells were incubated with fresh medium for 24 hours. Levels of osteocalcin (Alfa Aesar, Haverhill, MA) in the conditioned media were measured by ELISA according to the manufacturer's instructions, as described previously [1,2]. Cell layers were lysed and DNA, alkaline phosphatase specific activity, and protein levels were measured in the lysate (n=6). Alkaline phosphatase specific activity was normalized to total protein content of the cell layer lysates (BCA Protein Assay, Thermo Fisher), and levels of secreted factors in the conditioned media were normalized to DNA content (Quant-iT™ PicoGreen dsDNA Assay, Life Technologies).

### 4.2.4 Statistics

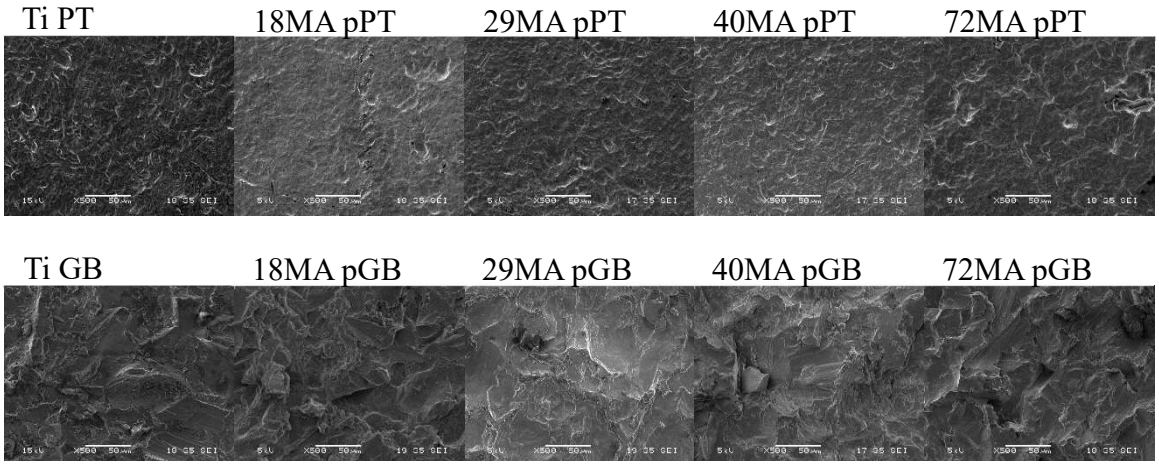


**Figure 4.2** SEM images of original Titanium discs and resultant MA-MMA discs.

Values are given are the mean ± SEM of six individual cultures per variable. Data were analyzed via analysis of variance (ANOVA) and when differences were detected, by post hoc analysis using Bonferonni's modification of Student's t-test. Significance was determined as $p < 0.05$.

### 4.3 Results

The surface topography carried to all stiffnesses well, apparent by SEM imagery (Figure 4.2). There were no statistical differences in roughness between the original titanium discs (Ti PT, Ti GB) and the resultant polymer discs (Figure 4.3), most evident

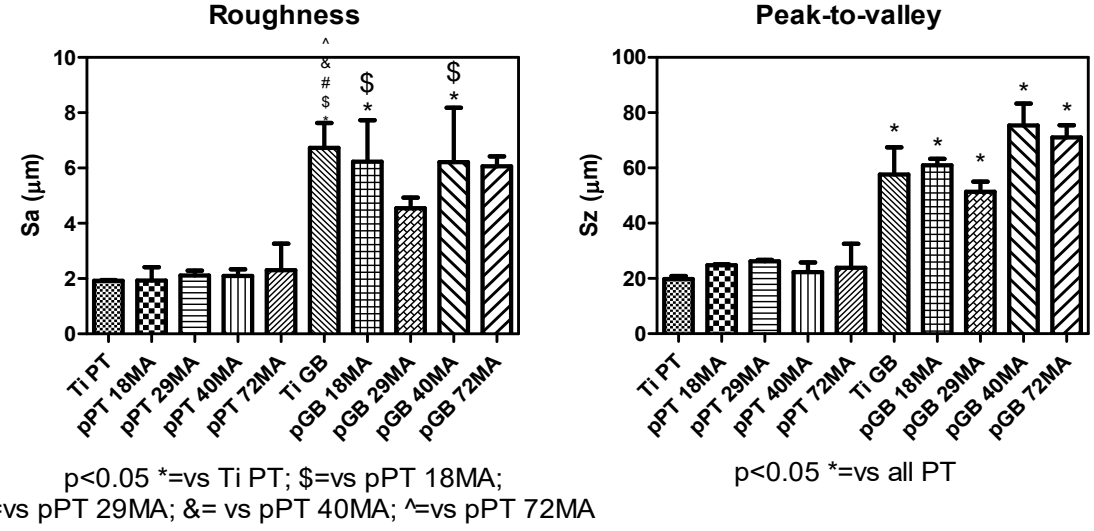


**Figure 4.3** Characterization of varied stiffness and roughness networks.

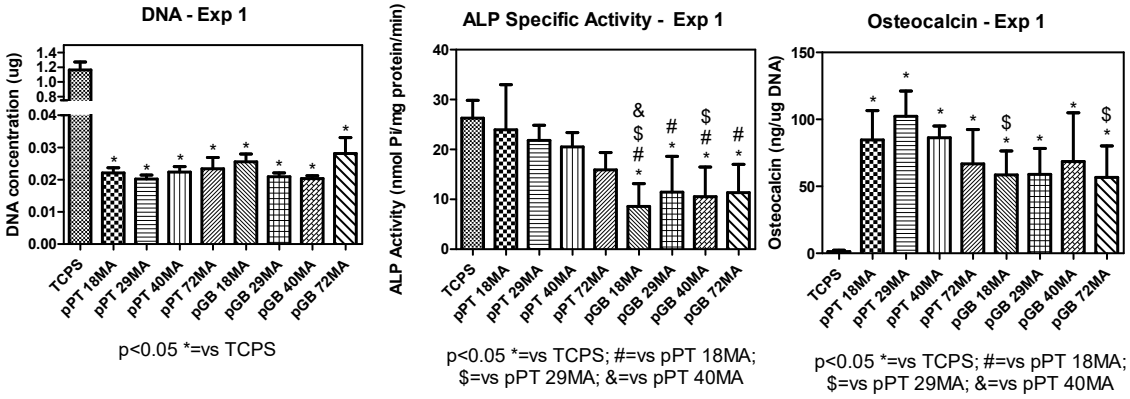


**Figure 4.4** MG63 cell behavior on varied stiffness and roughness networks.

in peak-to-vall ey height. MG63 cell DNA was reduced on polymer substrates compared to TCPS, but was not affected by surface topography (Figure 4.4). Alkaline phosphatase specific activity was reduced on the pGB groups compared to TCPS and pPT, however, this observation was not able to be reproduced. Neither was the apparent effect of an increase in osteocalcin from cells cultured on the polymer substrates able to be conclusively repeated.

## 4.4 Discussion

The data could not be repeated with respect to ALP specific activity and osteocalcin (the decrease in DNA was repeated, with no differences between pPT/pGB or the various stiffnesses, data not shown). While it is currently unknown why this occurred, one potential explanation is that the disc-to-disc variability was too high due to processing. However, we were again able to successfully transfer topography to these different stiffness polymers. If brought into more standard production, one could foresee using these unique materials to elucidate cell-surface interactions with respect to stiffness and roughness – for example, whether different pathways are used, similar integrins are involved, or if they can be completely decoupled.

# CHAPTER 5

# CONCLUSION

The work shown here demonstrates the feasibility of SMPs for biomedical use. The creation of a biocompatible SMP with 100% recovery at homeostatic temperature to a specific topography that influenced MG63 behavior is unique in the field. Current works focus predominantly on cell alignment on SMPs [60-62,75-78] and macroscopic shape changes for minimally invasive surgery [79,80]. While examination of cellular differentiation has been examined on some SMPs [81] there is a severe shortage of work looking at how dynamic topography can influence cell behavior. Others have seen phenomena associated with shape-change. For example, Gong, et. al., focused on elongation of rat bone marrow stromal cells to guide them down a myoblastic lineage rather than an osteoblastic lineage [82]. The work here helps to begin to fill the large gap in knowledge concerning osteoblasts and dynamic topography.

Dynamic topography is just one way of getting cells to do what we want. Another approach is to use scaffolds consisting of polymers with different degradation rates, which can be generated using a dual coaxial electrospinning device (Haifeng Chen, Peking University) (Appendix B, Figure B.1). These release rates in theory could match an MSC's normal progression into an osteoblast, giving a novel *in vitro* platform to look at osteogenesis in closer detail.

The method described in this thesis for creation of surface features on SMPs (in essence, soft lithography) is just one of many ways to do so. Depending on how one wants to influence cell behavior, one can imagine a myriad of random or specific surface arrangements. Other methods of creating surface features on SMPs include solvent casting [83] sputter coating (for wrinkles) [84] and domain-changing by stretching [85] or etching [86]. The incorporation of specific segments such as anti-biofouling [87], doping

with bio-relevant minerals such as hydroxyapatite [88], and further surface modification to include peptides known for cell homing such as E7, which has shown affinity for MSCs [89] could all be of benefit for SMPs in biomedical applications. In the case of further surface modification, however, one must take into account processing of the SMP. Depending on the nature of the modification, it may need to come after compression, but recovery of the SMP could then affect its placement on the surface – which may be desirable, or may not.

Another question that arises as this work is taken into account is the mechanisms by which osteoblasts sense this change in topography. How minute of a change would be necessary to achieve a similar outcome as one seen here? Examination of cell response to recovery over various timetables would be of interest, particularly since cells themselves exhibit some shape memory properties while undergoing division [90]. Future studies could also look into knockdown of specific integrins, or proteins involved in focal adhesion complexes or other cytoskeletal arrangements, to see what pathway(s) are at play [91-93]. Much is known regarding how cells sense stiffness at various levels (e.g. on the order of cartilage to on the order of cortical bone) but what is *not* known is whether they use similar mechanisms to sense roughness, and if so, which has more of an impact on cellular response – roughness, or stiffness? Do they synergize [94]? Or does the chemical makeup of the surface trump all [95]?

In conclusion, the ability to transfer rough topography onto various acrylate SMPs has been shown, as well as excellent recovery of rough BZA:BZMA:DDDMA networks under cell culture conditions. Furthermore, MG63 cells responded favorably in terms of quick increase in late osteoblast markers specifically on dynamic rough surfaces over static ones. Combinatory experiments of stiffness and roughness were unable to give conclusive results but warrant further investigation. Overall, the work presented here advances polymer chemistry for biomedical engineering applications.

# APPENDIX A

# SUBSTRATE STIFFNESS CONTROLS OSTEOBLASTIC AND CHONDROCYTIC DIFFERENTIATION OF MESENCHYMAL STEM CELLS WITHOUT EXOGENOUS STIMULI

## A.1 Introduction

Over six and a half million medical devices are implanted into Americans every year [96]. These devices have a wide array of mechanical, chemical, and morphological spectra. Many studies examining how these properties modulate differentiation of multipotent cells like mesenchymal stem cells (MSCs) have focused on a single lineage fate. Relatively little is known about how changes in the chemical and mechanical microenvironment of these cells might differentially modulate phenotypic expression along multiple lineages [97-100].

Several reports have shown that MSCs are sensitive to substrate properties, such as surface roughness, stiffness, chemistry, and energy, and differentiate along specific lineages in response to these cues [26,99,101-104]. In vivo, implant surface properties including roughness, chemistry, energy, and design affect bone-to-implant contact [105-107], in part by stimulating osteoblastic differentiation of MSCs during bone healing. In vitro studies show that these material surface properties can play a role in inducing MSC differentiation into osteoblasts in the absence of exogenous factors or media supplements [108-111]. However, the majority of these studies were performed on substrates with lower or higher moduli range than native moduli of bone where such biomaterials generally are placed [99]. Moreover, few studies have examined whether the effects of stiffness and

chemistry are unique to osteoblastic differentiation or if other mesenchymal lineage fates might be induced as well.

Cells use mechanoreceptors to detect substrate stiffness via a mechanism that involves integrin-dependent signaling [99]. We have shown that integrin expression in MSCs and osteoblasts is modulated by surface properties, with α5β1 being expressed on smooth titanium and titanium alloy substrates and α2β1 being expressed on microtextured surfaces. Whereas α5β1 is associated with attachment and proliferation [112], α2β1 signaling is required for osteoblast differentiation [113]. Integrin β1 has been shown to mediate effects of other material and environmental stimuli on cell response [114,115] and has been shown to play a role in chondrogenic differentiation [116,117].

In vivo, MSCs reside in tissues of varying stiffness and participate in tissue regeneration with stiffness changing as the repair tissue matures. This suggests that cells at different states within a lineage may respond differentially as they commit to a specific fate. To begin to examine this, we developed a series of polymer substrates with varying stiffness but without major changes in surface chemistry [37]. We found that a relatively high stiffness of 850 MPa was able to induce maturation of osteoblast-like MG63 cells. In the present study, we took advantage of methacrylate/methylmethacrylate polymer networks in which stiffness could be controlled by varying the amount of monomer, to investigate how stiffness mediates MSC commitment to two related lineages, osteogenic and chondrogenic, and compared MSC responses to those of committed osteoblasts and chondrocytes.

## A.2 Materials and Methods

*Polymer synthesis*. Polymer substrates with elastic moduli orders of magnitude apart were synthesized to examine the effects of stiffnesses in ranges beyond those

reported in current literature and with moduli relevant to clinical applications. To accomplish this, we varied the weight ratio of methyl acrylate (MA) and methyl methacrylate (MMA) crosslinked with 10% poly(ethylene glycol) dimethacrylate (PEGDMA). Copolymer solutions consisting of MA, MMA, and PEGDMA MW~750 were obtained from Sigma Aldrich and used as received. The weight ratio of MA to MMA was varied while the crosslinking concentration of PEGDMA was held constant at 10 wt% to produce four copolymer networks (by wt. % of MA): 18MA, 29MA, 40MA, and 72MA. 0.5 wt.% 2,2-dimethoxy-2-phenylacetophenone (DMPA) was used as the photoinitiator (Sigma-Aldrich). Co-monomer solutions were mixed manually and injected in between two 1 mm glass sheets. The samples were photopolymerized in a UV chamber (Model CL-1000L Ultraviolet Crosslinker; $\lambda = 365$nm) for 30 minutes. Discs were laser cut from the polymer sheets to fit into a well of a 24-well culture plate and UV sterilized for 90 minutes.

*Mechanical testing*. Tensile strain-to-failure tests to determine toughness and elastic modulus were performed on a universal testing machine (MTS Insight 2) using a 2kN load cell and a strain rate of 5%/s. ASTM D632 Type IV Dogbone samples were laser-cut with a 20 mm gauge length and 2.8 mm gauge width, and their edges were sanded to remove any laser-induced defects. Samples were soaked in phosphate buffered saline (PBS) for 24 hours prior to testing, removed from PBS, patted with a paper towel to remove excess PBS, and their dimensions measured using digital calipers. Following this, the samples were loaded in tensile grips, submerged in a PBS bath at 37°C, and held at 37°C for 10 min to allow for thermal equilibration.

Toughness was calculated as the area under the stress-strain curve in units of MJ/m3. Elastic modulus was determined by calculating the slope of the linear portion of the stress-strain curve (n=4). Dynamic mechanical analysis (DMA) in tensile loading was used to determine rubbery modulus of the networks corresponding to the degree of crosslinking (TA Q800 DMA, Newcastle, DE). Rectangular samples of 1 x 5 x 15 mm3

were laser cut from polymer sheets and their edges were sanded to remove any defects from the laser. The samples were thermally equilibrated at -75°C for 2 minutes and then heated to 200 °C at a rate of 5 °C/minute. Testing was performed in cyclic strain control at 0.2% strain with a preload force of 0.001 N and a force track setting of 150%. The glass transition temperature (Tg) was defined as the peak of the tan delta curve, and the rubbery modulus was measured as the storage modulus value taken 20°C beyond the lowest point in the rubbery plateau (n=3).

*Surface characterization*. Surface wettability was determined by performing contact angle measurements using the sessile drop method (Ramé-hart Model 250 goniometer, Mountain Lakes, NJ) (n=3). FTIR-ATR spectra were obtained on discs using a Bruker Optics Tensor Spectrometer (Billerica, MA) with a KBr crystal. Ten scans were obtained on each sample at a 1 Hz frequency and peak wavenumbers were determined using OMNIC software (Thermo Electron Corporation, Madison, WI). Three spectra were obtained for three separate discs for each composition.

*Cell studies*. Human MSCs and human osteoblasts (HOBs, Lonza) were obtained from Lonza (Walkersville, MO). Human auricular chondrocytes were isolated from pediatric ear cartilage obtained under an IRB approved protocol at Children's Hospital of Atlanta and Georgia Institute of Technology. Informed consent was from the guardian and was in written form. The chondrocytes were isolated as described previously [118], cultured to confluence and stored at -80˚C until used for this study. Cells in passage two were used for all studies. Expression of cartilage cell phenotype at this passage was verified by gene expression of SOX9, ACAN, COL2, and COMP (Supplemental Figure 1), as described in the following paragraph. We did not assess expression of mRNA for elastin, a marker of the auricular chondrocyte phenotype, as our intent was to examine the general properties of osteoblasts v. chondrocyte lineage commitment.

For the study, all cells were grown plated at a density of 10,000 cells/cm2 on copolymer surfaces and cultured in Dulbecco's modified Eagle's medium (CellGro® by

Mediatech, Manassas, VA) supplemented with 10% fetal bovine serum (Life Technologies, Carlsbad, CA) and 1% penicillin-streptomycin (Life Technologies). Cells were fed with this medium for 24 hours post-plating and every other day. After 7 days of culture, cells were incubated with fresh medium for 12 hours. RNA was isolated (TRIzol, Life Technologies) and quantified using a NanoDrop spectrophotometer (Thermo Scientific, Waltham, MA). To create a cDNA template, 500 ng of RNA was reverse transcribed using a High Capacity Reverse Transcription cDNA kit (Life Technologies). To quantify expression of RUNX2 mRNA in MSCs and HOBs, cDNA was used for real-time PCR with gene-specific primers (Supplemental Table 1) using the StepOnePlus Real-time PCR System and Power SYBR® Green PCR Master Mix (Life Technologies). Fluorescence values were quantified as starting quantities using known dilutions of cells cultured on tissue culture polystyrene (TCPS). mRNA expression was normalized to glyceraldehyde 3-phosphate dehydrogenase. Total cell number and cellular alkaline phosphatase specific activity were measured in the cell lysate as described previously [4].

Secreted osteocalcin (OCN, Biomedical Technologies, Stoughton, MA) and osteoprotegerin (R&D Systems, Minneapolis, MN) were measured to determine osteogenic differentiation. Immunoassays were normalized to total cell number. Chondrogenic differentiation was determined by measuring expression of mRNAs for aggrecan (ACAN), cartilage oligomeric matrix protein (COMP), and collagen type II (COL2) as described above. Cartilage matrix production was assessed using an Alcian blue assay (Sigma Aldrich, St. Louis, MO) to measure sulfated glycosaminoglycans. In brief, cell layers were fixed with 10% neutral buffered formalin for 10 minutes at room temperature. Cells were washed twice with PBS, then incubated with 3% acetic acid for 10 minutes. Proteoglycans were stained with 1% Alcian blue in 3% acetic acid (pH 2.5) for 30 minutes at room temperature. Cell layers were washed twice, and Alcian blue was extracted with dimethyl sulfoxide. Absorbance was measured at 650 nm [119].

For all experiments, MSCs, HOBs, and chondrocytes were grown at the same time with the same culture media to limit variability. To visualize cell shape, MSCs, HOBs and chondrocytes were plated on copolymer surfaces at a density of 5,000 cells/cm2 and allowed to spread for 24 hours in culture medium as described. Cell layers were fixed in 4% paraformaldehyde for 20 minutes and permeabilized in 0.05% Triton X-100 in PBS for 5 minutes. To visualize F-actin, cells were incubated for 1 hour with Alexa Fluor 488-labeled phalloidin (Life Technologies). At the end of the incubation period, cells were washed with PBS and incubated with Hoechst 33342 (Invitrogen) for 10 minutes. Finally, cultures were washed with 0.05% Triton X-100 in PBS, mounted on glass coverslips with Fluoro-Gel with Tris buffer (Electron Microscopy Sciences, Hatifield, PA) and imaged (Zeiss LSM 510 NLO with META MPE, Carl Zeiss Microscopy, Thornwood, NY).

To examine integrin expression, MSCs, HOBs, and chondrocytes were plated on copolymer surfaces at a density of 10,000 cells/cm2 on copolymer surfaces and cultured in the same culture medium as described above. Cells were fed 24 hours post-plating and every other day thereafter. After 7 days, cells were incubated with fresh media for 12 hours and gene expression for integrins α1, α2, α5, αv, β1, and β3 measured as described above.

Permanently silenced ITGB1 MSCs were generated to examine integrin-dependent MSC differentiation on surfaces of varying stiffness. MSCs were transduced with shRNA lentiviral transduction particles (SHCLNV_NM_002211, TRCN 0000029645, Mission®, Sigma Aldrich) to silence ITGB1. MSCs plated at 20,000 cells/cm2 were cultured overnight. Cells were incubated with particles (multiplicity of infection 5.0) overnight. Transduced cells were selected with culture media containing 0.25 μg/ml puromycin, yielding cells with 85% knockdown of mRNA. Quantification of mRNA levels of SOX9 and RUNX2, cell number, alkaline phosphatase specific activity, and secreted OCN and OPG were performed as described above.

*Statistics*. Data are shown as mean +/- SEM of six independent cultures from a representative experiment. All experiments were repeated. Using ANOVA with post-hoc Bonferroni's modification of Student's t-test a value of $P < 0.05$ was considered statistically significant.

## A.3 Results

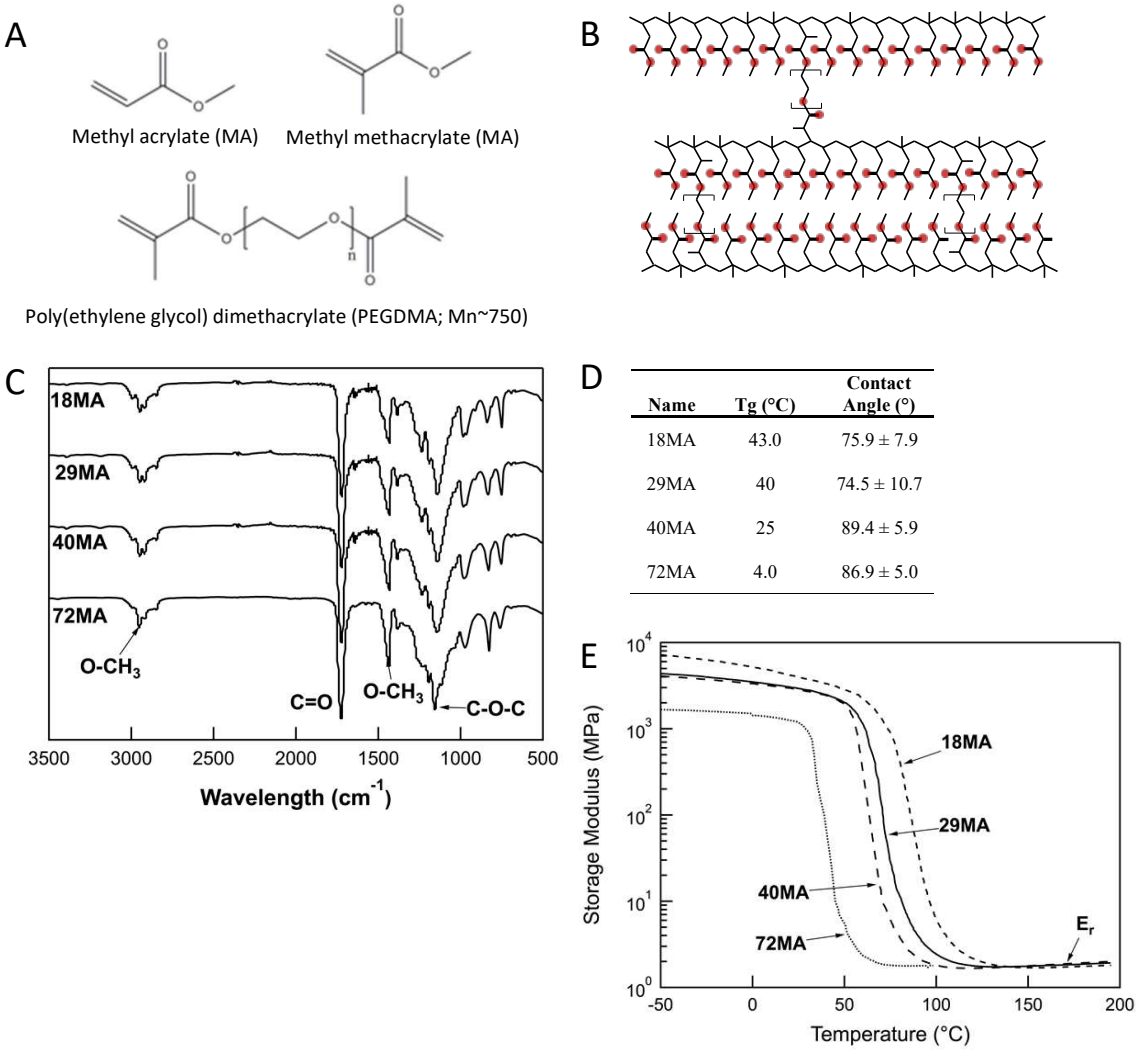


**Figure A.1**. Characterization of MA-MMA networks. (A) Monomers used to create networks of increasing stiffness. (B) Example of crosslinked network. (C) Representative FTIR-ATR spectra for each network indicating similar surface chemistry for each. (D) Glass transition temperature (Tg) and contact angle of crosslinked networks. (E) DMA of crosslinked networks (n=3).

The similar chemical makeup of the monomers (Fig. A.1A) yielded networks (Fig. A.1B) with similar surface chemistries as indicated by their FTIR-ATR spectra – the position of the major bonds (O-CH3, C=O, and C-O-C) did not shift between the different compositions (Fig. A.1C). Although these networks had similar surface energy as evidenced by similar contact angles (Fig. A.1D), their elastic moduli, measured in PBS at 37°C, spanned multiple orders of magnitude, (18MA>29MA>40MA>72MA) (Fig. A.1E). The toughness of the MA-MMA copolymers closely mimics the reported toughness of hard biological tissues including dentin and cortical bone (Fig. A.2).

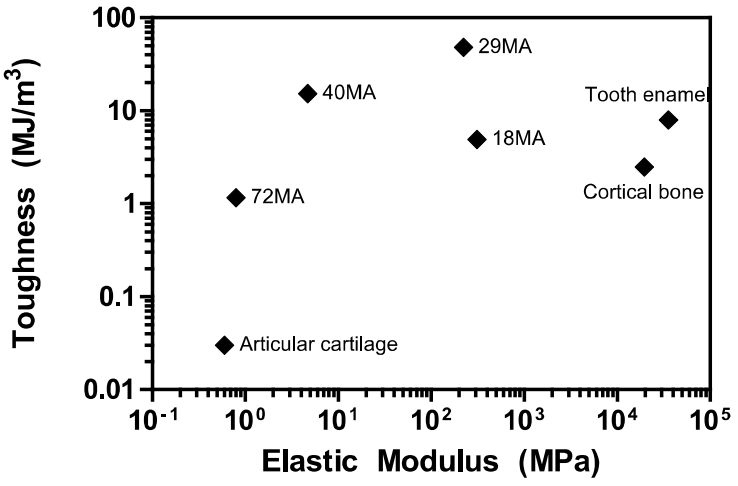


| Name | 18MA | 29MA | 40MA | 72MA |
|---|---|---|---|---|
| E (MPa) | 309.9 ± 6.5 | 223.7 ± 31.5 | 4.7 ± 1.0 | 0.8 ± 0.1 |

Max

**Figure A.2**. Toughness vs. elastic modulus for load-bearing biological tissues (green) and MA-MMA networks (black). Modified from data from Ref [24].

Stiffness affected the structural organization of cytoskeletal filaments. MSCs grown on MA-MMA copolymer surfaces were longer on the less stiff surfaces, with multiple contact points on the 40MA surface (Fig. A.3A-D). Unlike MSCs grown on surfaces with lower stiffness, F-actin appeared to be reduced in MSCs grown on 18MA surfaces (Fig. A.3A). HOBs were noticeably smaller on the 18MA surface (Fig. A.3E) and more spread out on the less stiff surfaces (Fig. A.3F-H). Chondrocytes on 18MA, 29MA, and 40MA had similar morphology with long extensions and few points of contact (Fig. A.3I-K), and began to spread wider on the least stiff surface (Fig. A.3L). However, the pattern of F-actin

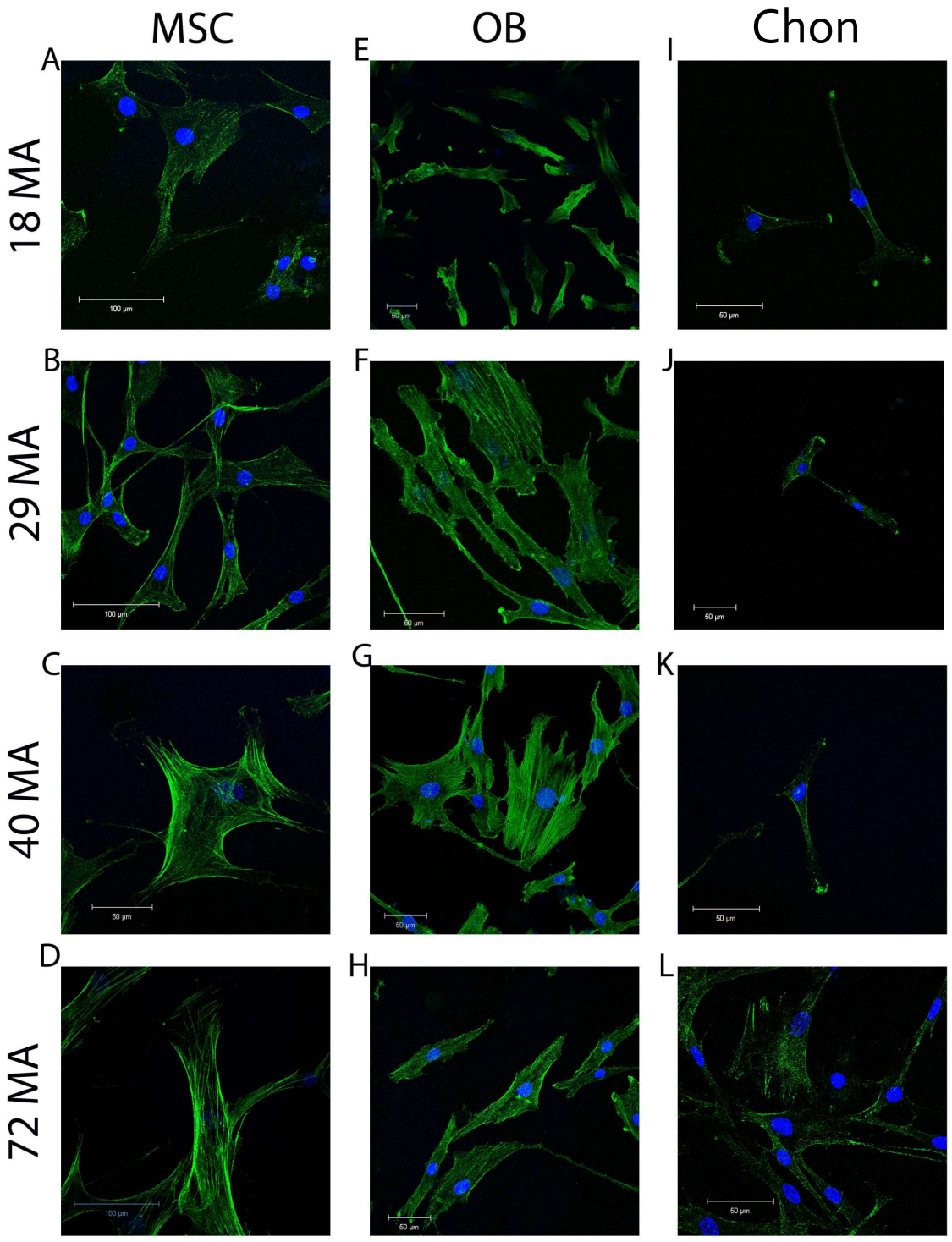


**Figure A.3**. Stiffness-dependent cytoskeleton arrangement. Representative staining of F-actin by phalloidin (green) and nuclei by DAPI (blue) in human MSCs (A-D), HOBs (E-H), and chondrocytes (I-L) cultured on surfaces of varying stiffness. (Scale bars: 100 µm for A,B,D; 50 µm for all others.)

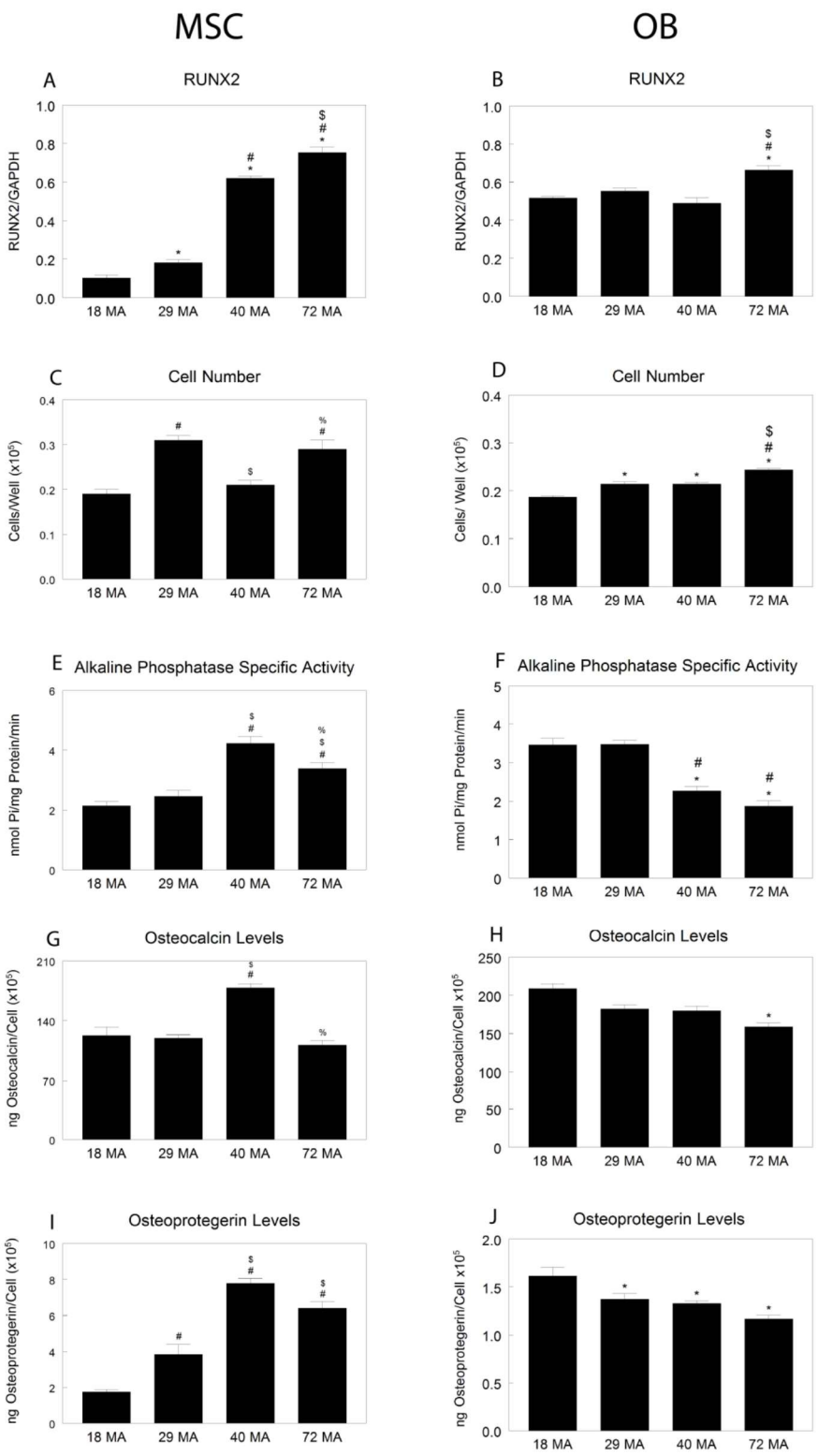


**Figure A.4**. Osteoblastic differentiation on MA-MMA networks. (A-B) mRNA levels for osteoblast-specific marker RUNX2. (C-J) MSC and HOB response to substrate stiffness seen in cell number and osteogenic protein levels. *P < 0.05 vs. 18 MA, #P <0.05 vs. 29 MA, $P <0.05 vs. 40 MA.

organization was not changed in a stiffness-dependent manner for HOBs and

chondrocytes (Fig. A.3E-L).

We then compared the effects of stiffness on osteoblast phenotype in mMSCs and mature osteoblasts. MSCs and HOBs were grown without exogenous growth factors typically used to induce differentiation (see materials and methods). mRNA levels of transcription factor RUNX2 showed MSCs were more sensitive to stiffness than osteoblasts. RUNX2 increased in a stiffness-dependent manner in MSCs that was not present in OBs; however, the highest RUNX2 levels were seen on 72MA surfaces in both cell types (Fig. A.4A-B). Cell number was significantly higher on the 29MA and 72MA surfaces for MSCs whereas in HOBs peak numbers were found on 72MA, followed by 29MA and 40MA (Fig. A.4C-D). Alkaline phosphatase specific activity, an early marker for cells in the osteoblast lineage, was greatest in MSCs grown on 40MA followed by 72MA while HOBs grown on these stiffnesses had lower alkaline phosphatase activity compared to 18MA (Fig. A.4E-F). mRNAs for matrix proteins osteocalcin and osteoprotegerin, associated with more mature osteoblasts, were similarly affected. Peak levels of these proteins occurred in MSCs grown on 40MA (Fig. A.4G,I). Conversely, there was a decrease in osteocalcin expression in HOBs grown on the least stiff substrates (Fig. A.4H), and osteoprotegerin mRNAs were lower in HOBs grown on all but 18MA (Fig. A.4J).

Chondrogenic differentiation of MSCs and chondrogenic markers in chondrocytes were responsive to substrate stiffness as well. MSCs and chondrocytes were grown for 7 days on the polymer surfaces without exogenous growth factors to induce differentiation (see materials and methods). SOX9, ACAN, COMP, and COL2 all increased in a stiffness-dependent manner for MSCs and were greatest on 72MA (Fig. A.5A,C,E,G) whereas levels of SOX9 were equally high in chondrocytes grown on 40MA and 72MA (Fig. A.5B). ACAN levels in chondrocytes mimicked MSCs for 40MA and 72MA (Fig. A.5C-D), but contrary to MSCs the level of COMP decreased on those same surfaces (Fig. A.5E-F). There was a stiffness-dependent increase in the level of COL2 for

chondrocytes, however, similar to MSCs (Fig. A.5G-H). Sulfated glycosaminoglycan

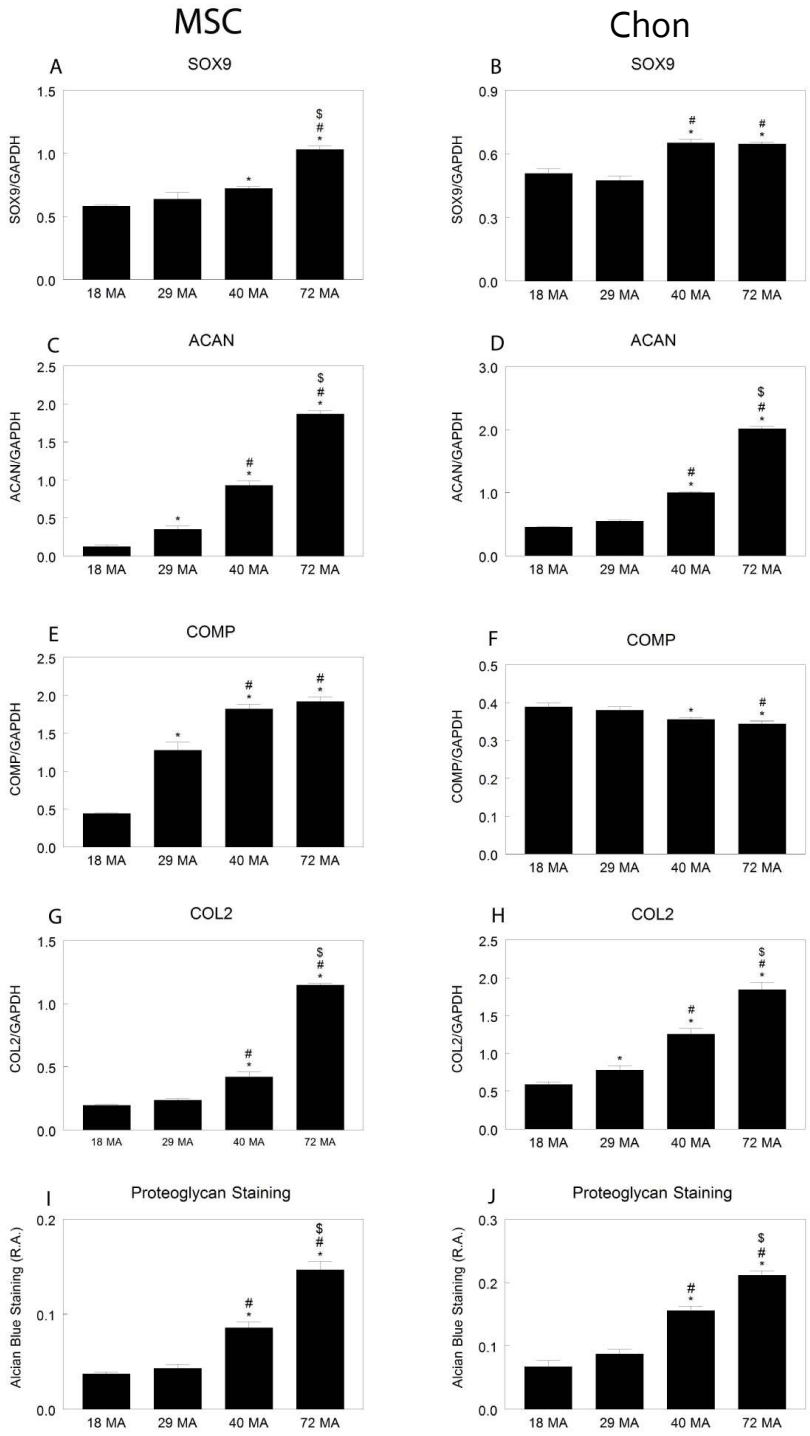


**Figure A.5**. Chondrogenic differentiation on MA-MMA networks. Levels of chondrogenic mRNA (A-H) and quantification of proteoglycan staining in MSCs and chondrocytes (I-J) cultured on surfaces of varying stiffness. *P < 0.05 vs. 18 MA, #P <0.05 vs. 29 MA, $P <0.05 vs. 40 MA.

staining by Alcian blue was similar for both MSCs and chondrocytes in that there was an increase in staining in cells grown on both 40MA and 72MA surfaces with the greatest intensity in cells grown on the least stiff surface (Fig. A.5I-J).

Integrin expression was surface-dependent in all three cell types after seven days in culture. In MSCs, levels of ITGA1 and ITGA2 were higher on 29MA and 72MA substrates than on 18MA, with peak levels occurring in MSCs grown on the 40MA (4.7 MPa stiffness, Fig. A.6A-B). A stiffness-dependent increase in the mRNA levels of ITGA5 and ITGB1 was seen in MSCs, with higher levels in MSCs grown on the least stiff surfaces (Fig. A.6C,E). Levels of IGTAV were significantly higher only on the 40MA and 72MA surfaces, peaking on the 40MA surfaces (Fig. A.6D). Conversely, a stiffness-dependent decrease in the levels of ITGB3 was seen on the surfaces (Fig. A.6F). In HOBs, ITGA1 levels were higher on all but the most stiff surface, peaking on the 40MA (Fig. A.6G), but levels of ITGA2 were highest in cells grown on 29MA and lower in those grown on the copolymers with lower stiffness (Fig. A.6H). HOBs grown on the surfaces with lower stiffness had higher levels of ITGA5 but lower levels of ITGAV (Fig. A.6I-J). The mRNA level for ITGB1 in HOBs was lowest on the stiffest surface (Fig. A.6K). A decrease in the levels of ITGB3 could be seen for HOBs grown on both 40MA and 72MA surfaces with the greatest decrease from those on the least stiff surface (Fig. A.6L). Finally, in chondrocytes, ITGA1 mRNAs increased in cells grown on the 40MA surface with higher levels in those grown on the 72MA surface (Fig. A.6M). The levels of ITGA2 were lower in chondrocytes grown on surfaces with lower stiffness (Fig. A.6N). Chondrocytes had similar levels of ITGA5 on all surfaces, but were significantly higher from those grown on the least stiff surface (Fig. A.6O). The levels of both ITGAV and ITGB1 increased in chondrocytes grown on surfaces with lower stiffness (Fig. A.6P,Q) and, as in MSCs, a similar stiffness-dependent decrease in the level of ITGB3 was observed (Fig. A.6R).

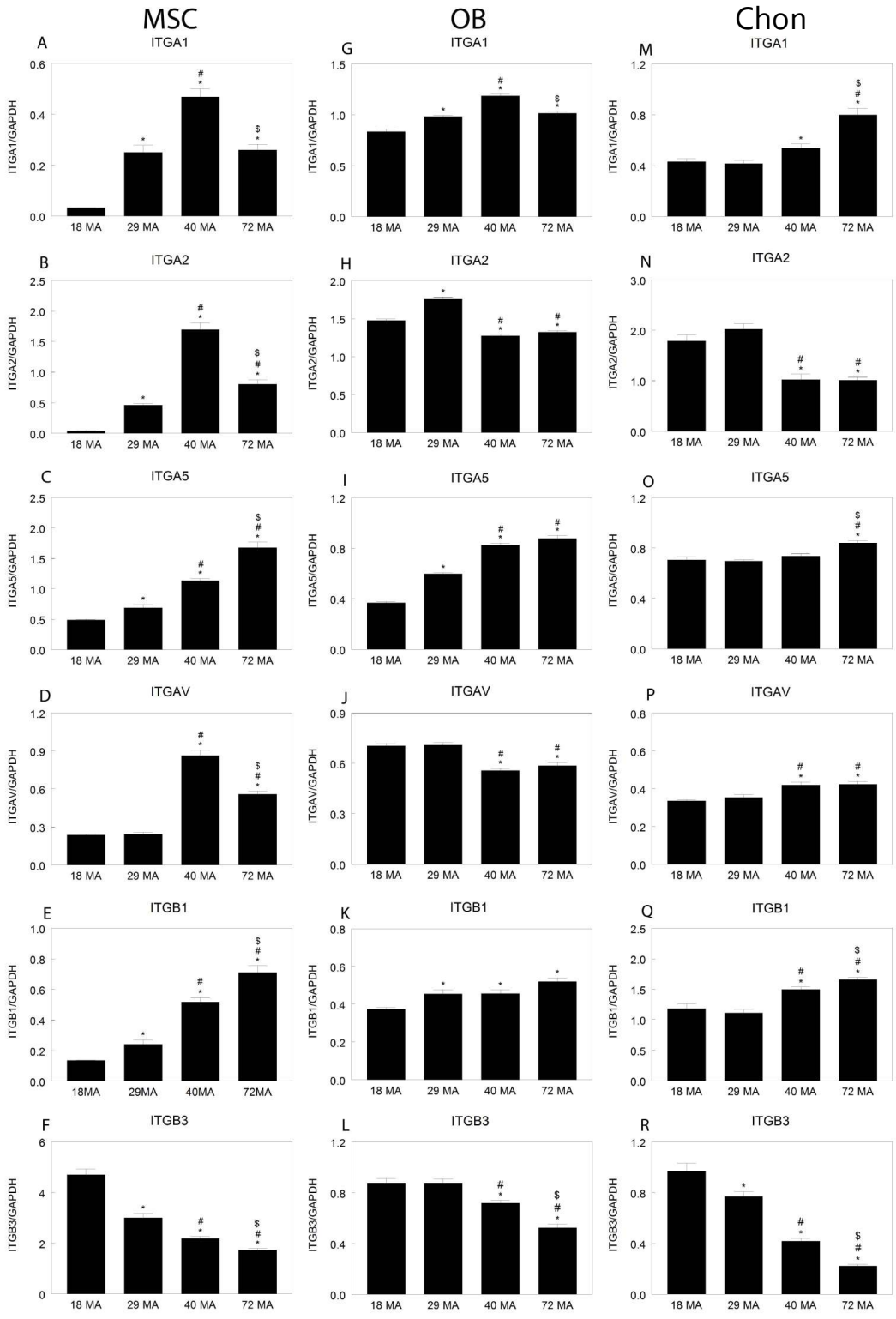


**Figure A.6**. Integrin expression is stiffness- and cell-type- dependent. Comparison of integrin mRNA levels in MSCs, OBs, and chondrocytes cultured on surfaces of varying stiffness. *P < 0.05 vs. 18 MA, #P <0.05 vs. 29 MA, $P <0.05 vs. 40 MA.

Because MSCs tended to be the most sensitive to the varied stiffness, we wanted

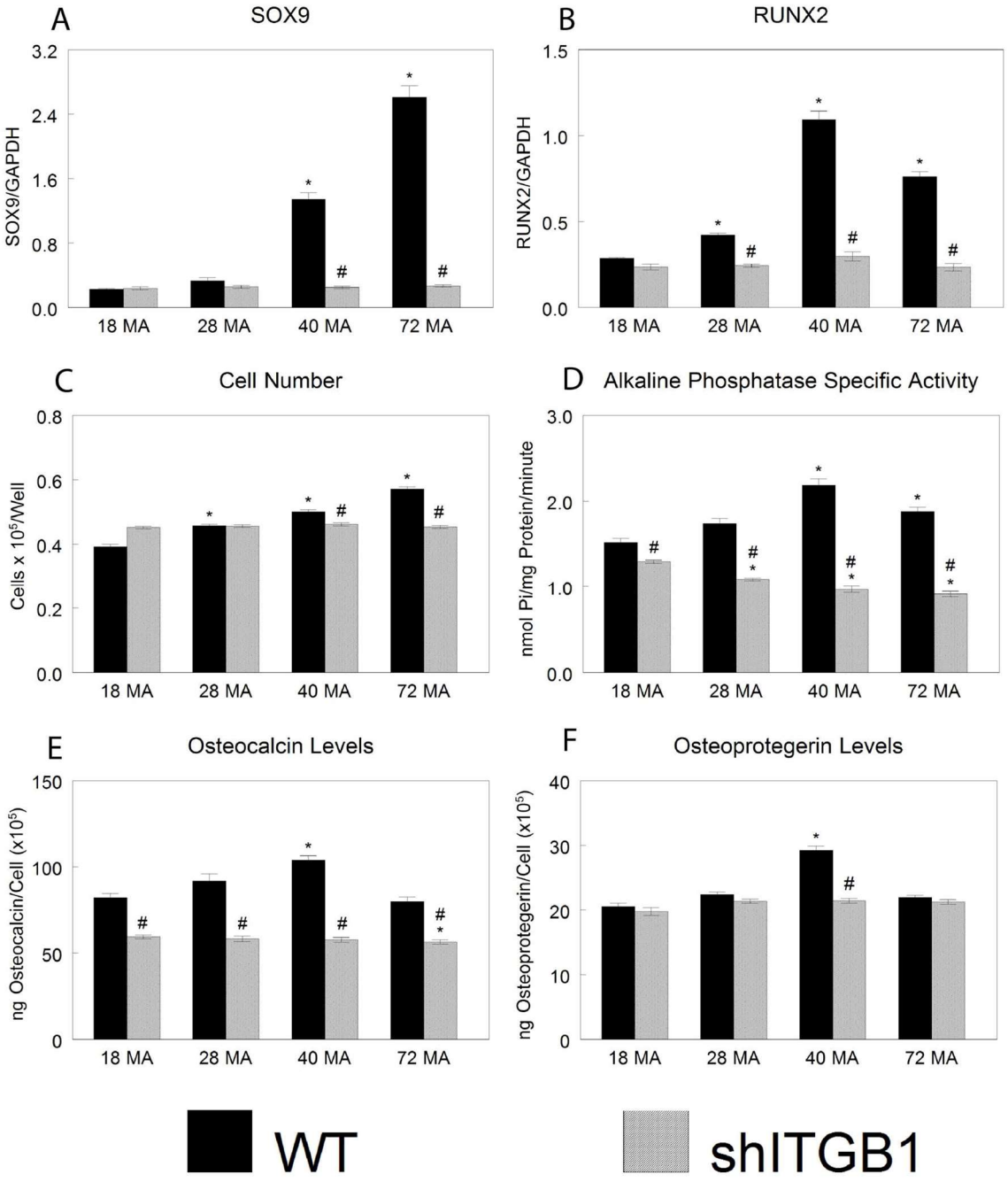


**Fig A.7**. Integrin-dependent osteoblast differentiation. Levels of chondrogenic (A) and osteoblastic (B) mRNA. (C-F) Cell number and osteogenic protein levels in wild type human MSCs (WT) and silenced integrin β1 MSCs (shITGB1) cultured on surfaces of varying stiffness. *P < 0.05 vs. 18 MA, #P <0.05 vs. wild type.

to determine how silencing integrin β1 (ITGB1) in these cells would modulate this response. Silencing ITGB1 abolished the stiffness-dependent increase in mRNA levels of transcription factors for chondrocytes (SOX9) and osteoblasts (RUNX2) (Fig. A.7A-B).

Silencing ITGB1 also abolished the increase in cell number on decreasingly stiff surfaces seen in WT MSCs (Fig. A.7C). shITGB1-MSCs had lower alkaline phosphatase specific activity compared to their wild-type counterparts and the levels decreased with decreasing stiffness (Fig. A.7D). Osteocalcin levels that were highest on 40MA in WT MSCs were lower in the silenced cells on all stiffnesses and lowest on 72MA surfaces (Fig. A.7E). Finally, the increase of osteoprotegerin in wild type cells grown on 40MA was also abolished in shITGB1-MSCs (Fig. A.7F).

## A.4 Discussion

Multipotent stem cells from various sources have previously been shown to differentiate in response to varying topographies and stiffnesses [26,31,120-122]. In most cases, this differentiation has been enhanced with different induction media resulting in a very complex process that potentially masks effects of surface features, chemistry, or stiffness. In our study, we eliminated all but one of these variables, stiffness, in order to tease out its effects on MSC differentiation along two lineage fates: chondrogenic and osteogenic. Our results show that stiffness alone is able to direct differentiation and that different stiffnesses favor expression of a cartilage cell phenotype v. expression of an osteoblast phenotype, but no one stiffness produces an exclusive outcome.

We did not observe significant morphological changes in MSCs, HOBs, or chondrocytes on our polymer networks as others have demonstrated [26,123] although we did see some stiffness-dependent cytoskeletal arrangement. Significant changes in expression of differentiation markers do not necessarily correlate with outward changes in MSC morphology over the short time course of our study [124]. Similarly, we did not observe morphological changes in the chondrocyte and osteoblast cultures, although gene expression for differentiation markers was affected.

Gene expression in the cultures did vary with cell type and with substrate stiffness. MSCs exhibited increasing RUNX2 expression with decreasing stiffness,

whereas expression in the committed HOB cells was less sensitive to substrate. Levels of this factor are correlated with osteoblastic differentiation of MSCs [125-127], suggesting that less stiff substrates induced osteoblastic differentiation. Whether this reflects in vivo differentiation on osteoclast resorbed bone surfaces, which are primarily collagen and non-collagenous proteins like osteopontin rather than stiffer fully mineralized bone [128,129], isn't clear.

We had expected MSCs to behave more like HOBs on the stiffer surface and more like chondrocytes on the less stiff surfaces but MSC responses were observed on the less stiff polymers (40MA and 72MA) for both lineages, indicating a mixed population exhibiting both osteoblastic and chondrogenic markers: more osteoblastic markers on the slightly less soft surface and more chondrogenic markers on the softest surface. The observation that MSCs had the highest osteoblast response on the next to least stiff (40MA) networks and the highest chondrogenic response on the least stiff (72MA) networks is an indicator that there exists an optimal substrate stiffness to promote osteoblast differentiation and that it is not simply 'the harder, the better.'

HOB expression levels of osteoblastic genes increased only on the stiffer surfaces; on the softer surfaces they not only didn't have this increase but may have begun to dedifferentiate. This suggests that maintenance of an osteoblastic phenotype may require a stiffer microenvironment typical of mineralized bone. To achieve a stable osteoblast phenotype in MSCs grown on TCPS requires extensive time in culture to develop multi-layered nodules and generally requires the use of media supplements for as long as 3 weeks to support mineral formation within the nodules [130]. Our study did not examine the long-term effects of MSCs on the softer 72MA substrate to determine if stiffness alone would support stable osteoblastic differentiation and matrix mineralization. Continued culture on the softer substrate in the absence of media supplements could have an inhibitory effect on downstream osteoblastic differentiation.

The differentiated HOBs behaved differently than the MSCs on the varied stiffnesses, suggesting that as differentiation progresses, substrate stiffness continues to influence cell maturation. Metal and ceramic implants generally have moduli much higher than native bone; any polymer scaffold or bone substitute must take stiffness into account as a critical factor. Most published work examining cell response to substrate stiffness use polymers such as hydrogels, which have moduli orders of magnitude lower than 100 kPa, far below biological tissues such as dental tissue or cortical bone, which are at or near common implant sites [115,120,121,131-133]. In contrast, chondrocytes, which exist in a hydrogel environment in vivo [134] behaved very similarly to MSCs.

Our results indicate that differential expression of integrins in response to surface stiffness plays a crucial role in determining cell response, and that MSC differentiation is controlled by integrin signaling. Because integrins are a cell's primary response to substrate stiffness due to ligand binding [100,135,136], and change according to differentiation [137], it follows that depending on a cell's phenotype it would have more or less sensitivity to substrate stiffness. Expression of ITGA1, ITGA2, and ITGA5 in particular in MSCs was much more sensitive to stiffness than in either osteoblasts or chondrocytes. Others have reported a similar increase in ITGA5 in murine fibroblasts though no substrates stiffer than 55 kPa were examined [136]. Izal-Azcarate et al. looked at integrin expression in rat chondrocytes on surfaces of 2-20 Pa stiffness under normoxia and hypoxia conditions and saw a decrease in ITGA2 and ITGAV, but no differences in ITGA1, ITGB1, or ITGB3 under normoxia [100], whereas we did. The softness of the substrates examined could account for the difference in our data compared to theirs, as changes in ITGB3 expression were not seen until MSCs were grown on stiffer substrates. The silencing of ITGB1 completely abolished this sensitivity at one week, faster than the 2-3 weeks reported previously [135]. The abolition of the SOX9 response in MSCs by ITGB1 silencing is likely due to cellular stiffness and diffusion changes, as others have seen increased activation of ITGB1 on softer substrates [114,138].

## A.5 Conclusion

Our results show that stiffness can direct the fate of MSCs and suggest that over a very small range, induce bone or cartilage formation – or both, such as our 40MA networks, which showed an enhancement of bone and cartilage markers. Once cells commit to an osteoblast lineage, stiffness has a completely different effect, suggesting that softer substrates could halt further osteoblast maturation. We were able to enhance chondrocyte markers in mature chondrocytes while the same networks inhibited osteoblast markers in mature osteoblasts. In addition we show that multiple integrins and integrin □1 in particular play a key role in MSC sensitivity to stiffness. Understanding the importance of this mechanical property unlocks its useful potential for exploitation in order to control cell fate.

# APPENDIX B

# DUAL COAXIAL ELECTROSPINNING

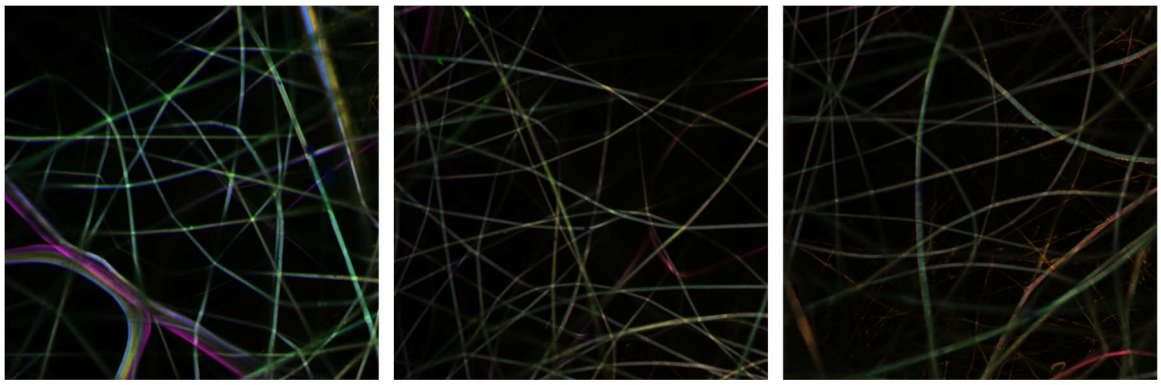

**Figure B.1** Dual coaxial electrospinning. Core 1 was 15% polyvinylpyrrolidone (PVP) in *N,N*-dimethylformamide (DMFA) mixed with rhodamine at a rate of 0.1mL/hr. Core 2 was 10% PVP in DMFA mixed with fluorescein at a rate of 0.11 mL/hr. Shell was 25% polycaprolactone (PCL) in DMFA mixed with Nile Blue A at a rate of 0.25 mL/hr. Distance between needle tip and mat was approximately 15 cm. Voltage was around 10 kV. Images taken on a Zeiss LSM-710.

# REFERENCES


1. Caicedo M, M.D., Jacobs JJ, M.D., Hallab NJ, M.D. Inflammatory bone loss in joint replacements: The mechanisms. The Journal of Musculoskeletal Medicine 2010;27:209-212-215-216.

2. Lucintel Forecasts Moderate Growth for the Global Passive Component Industry During 2013-2018. PRWeb.com Press Release Feed - PRWeb Press Release Account Feed 2013.

3. Anner R, Grossmann Y, Anner Y, Levin L. Smoking, diabetes mellitus, periodontitis, and supportive periodontal treatment as factors associated with dental implant survival: a long-term retrospective evaluation of patients followed for up to 10 years. Implant Dent 2010;19:57-64.

4. Olivares-Navarrete R, Raines AL, Hyzy SL, Park JH, Hutton DL, Cochran DL, et al. Osteoblast maturation and new bone formation in response to titanium implant surface features are reduced with age. J Bone Miner Res 2012;27:1773-1783.

5. Smith KE, Sawicki S, Hyjek MA, Downey S, Gall K. The effect of the glass transition temperature on the toughness of photopolymerizable (meth)acrylate networks under physiological conditions. Polymer (Guildf) 2009;50:5112-5123.

6. Yakacki CM, Shandas R, Safranski D, Ortega AM, Sassaman K, Gall K. Strong, tailored, biocompatible shape-memory polymer networks. Adv Funct Mater 2008;18:2428-2435.

7. Mather PT, Luo X, Rousseau IA. Shape memory polymer research. Annu Rev Mater Res 2009;39:445-471.

8. Leng J, Lan X, Liu Y, Du S. Shape-memory polymers and their composites: Stimulus methods and applications. Progress in Materials Science 2011;56:1077-1135.

9. Huang L, Zhuang X, Hu J, Lang L, Zhang P, Wang Y, et al. Synthesis of biodegradable and electroactive multiblock polylactide and aniline pentamer copolymer for tissue engineering applications. Biomacromolecules 2008;9:850-858.

10. Nelson BA, King WP, Gall K. Shape recovery of nanoscale imprints in a thermoset “shape memory” polymer. Appl Phys Lett 2005;86:103108.

11. Ortega AM, Yakacki CM, Dixon SA, Likos R, Greenberg AR, Gall K. Effect of crosslinking and long-term storage on the shape-memory behavior of (meth)acrylate-based shape-memory polymers. Soft Matter 2012;8:7381.

12. Lakhera N, Yakacki CM, Nguyen TD, Frick CP. Partially constrained recovery of (meth)acrylate shape-memory polymer networks. J Appl Polym Sci 2012;126:72-82.

13. Lendlein A, Langer R. Biodegradable, elastic shape-memory polymers for potential biomedical applications. Science 2002;296:1673-1676.

14. Tamai H, Igaki K, Kyo E, Kosuga K, Kawashima A, Matsui S, et al. Initial and 6-Month Results of Biodegradable Poly-l-Lactic Acid Coronary Stents in Humans. Circulation 2000;102:399-404.

15. Maitland DJ, Metzger MF, Schumann D, Lee A, Wilson TS. Photothermal properties of shape memory polymer micro-actuators for treating stroke. Lasers Surg Med 2002;30:1-11.

16. Small W, Wilson TS, Benett WJ, Loge JM, Maitland DJ. Laser-activated shape memory polymer intravascular thrombectomy device. Optics Express 2005;13:8204.

17. Nakasima A, Hu JR, Ichinose M, Shimada H. Potential application of shape memory plastic as elastic material in clinical orthodontics. The European Journal of Orthodontics 1991;13:179-186.

18. Lantada AD, Del Valle-Fernández R, Morgado PL, Muñoz-García J, Sanz JLM, Munoz-Guijosa J, et al. Development of Personalized Annuloplasty Rings: Combination of CT Images and CAD-CAM Tools. Ann Biomed Eng 2010;38:280-290.

19. Sharp AA, Panchawagh HV, Ortega A, Artale R, Richardson-Burns S, Finch DS, et al. Toward a self-deploying shape memory polymer neuronal electrode. Journal of Neural Engineering 2006;3:L23-L30.

20. Takehara H, Jiang C, Uto K, Ebara M, Aoyagi T, Ichiki T. Novel Microfluidic Valve Technology Based on Shape Memory Effect of Poly(e-caprolactone). Applied Physics Express 2013;6:037201.

21. Wong YS, Salvekar AV, Zhuang KD, Liu H, Birch WR, Tay KH, et al. Bioabsorbable radiopaque water-responsive shape memory embolization plug for temporary vascular occlusion. Biomaterials 2016;102:98-106.

22. Jing X, Mi HY, Huang HX, Turng LS. Shape memory thermoplastic polyurethane (TPU)/poly(epsilon-caprolactone) (PCL) blends as self-knotting sutures. J Mech Behav Biomed Mater 2016;64:94-103.

23. Yakacki CM, Shandas R, Lanning C, Rech B, Eckstein A, Gall K. Unconstrained recovery characterization of shape-memory polymer networks for cardiovascular applications. Biomaterials 2007;28:2255-2263.

24. Lian JB, Stein GS. Concepts of osteoblast growth and differentiation: basis for modulation of bone cell development and tissue formation. Crit Rev Oral Biol Med 1992;3:269-305.

25. Chen Q, Shou P, Zheng C, Jiang M, Cao G, Yang Q, et al. Fate decision of mesenchymal stem cells: adipocytes or osteoblasts. Cell Death Differ 2016;23:1128-1139.

26. Engler AJ, Sen S, Sweeney HL, Discher DE. Matrix elasticity directs stem cell lineage specification. Cell 2006;126:677-689.

27. Kilian KA, Bugarija B, Lahn BT, Mrksich M. Geometric cues for directing the differentiation of mesenchymal stem cells. Proc Natl Acad Sci U S A 2010;107:4872-4877.

28. D'Angelo F, Armentano I, Mattioli S, Crispoltoni L, Tiribuzi R, Cerulli GG, et al. Micropatterned hydrogenated amorphous carbon guides mesenchymal stem cells towards neuronal differentiation. Eur Cell Mater 2010;20:231-244.

29. Martino S, D'Angelo F, Armentano I, Kenny JM, Orlacchio A. Stem cell-biomaterial interactions for regenerative medicine. Biotechnol Adv 2012;30:338-351.

30. Lutolf MP, Hubbell JA. Synthetic biomaterials as instructive extracellular microenvironments for morphogenesis in tissue engineering. Nat Biotechnol 2005;23:47-55.

31. Martin JY, Schwartz Z, Hummert TW, Schraub DM, Simpson J, Lankford J,Jr, et al. Effect of titanium surface roughness on proliferation, differentiation, and protein synthesis of human osteoblast-like cells (MG63). J Biomed Mater Res 1995;29:389-401.

32. Kim MJ, Kim CW, Lim YJ, Heo SJ. Microrough titanium surface affects biologic response in MG63 osteoblast-like cells. J Biomed Mater Res A 2006;79:1023-1032.

33. Sul YT, Kang BS, Johansson C, Um HS, Park CJ, Albrektsson T. The roles of surface chemistry and topography in the strength and rate of osseointegration of titanium implants in bone. J Biomed Mater Res A 2009;89:942-950.

34. Lee EM, Smith KE, Gall K, Boyan BD, Schwartz Z. Change in surface roughness by dynamic shape-meemory acrylate networks enhances osteoblast differentiation. Biomaterials 2016.

35. Wong JY, Leach JB, Brown XQ. Balance of chemistry, topography, and mechanics at the cell–biomaterial interface: Issues and challenges for assessing the role of substrate mechanics on cell response. Surf Sci 2004;570:119-133.

36. Rolli CG, Nakayama H, Yamaguchi K, Spatz JP, Kemkemer R, Nakanishi J. Switchable adhesive substrates: revealing geometry dependence in collective cell behavior. Biomaterials 2012;33:2409-2418.

37. Smith KE, Hyzy SL, Sunwoo M, Gall KA, Schwartz Z, Boyan BD. The dependence of MG63 osteoblast responses to (meth)acrylate-based networks on chemical structure and stiffness. Biomaterials 2010;31:6131-6141.

38. Anselme K. Osteoblast adhesion on biomaterials. Biomaterials 2000;21:667-681.

39. Mendonca DB, Miguez PA, Mendonca G, Yamauchi M, Aragao FJ, Cooper LF. Titanium surface topography affects collagen biosynthesis of adherent cells. Bone 2011;49:463-472.

40. Impellitteri NA, Toepke MW, Lan Levengood SK, Murphy WL. Specific VEGF sequestering and release using peptide-functionalized hydrogel microspheres. Biomaterials 2012;33:3475-3484.

41. Hanjaya-Putra D, Wong KT, Hirotsu K, Khetan S, Burdick JA, Gerecht S. Spatial control of cell-mediated degradation to regulate vasculogenesis and angiogenesis in hyaluronan hydrogels. Biomaterials 2012;33:6123-6131.

42. Sedaghati T, Jell G, Seifalian A. Investigation of Schwann cell behaviour on RGD-functionalised bioabsorbable nanocomposite for peripheral nerve regeneration. N Biotechnol 2014;31:203-213.

43. Polte TR, Shen M, Karavitis J, Montoya M, Pendse J, Xia S, et al. Nanostructured magnetizable materials that switch cells between life and death. Biomaterials 2007;28:2783-2790.

44. Zhang W, Wang G, Liu Y, Zhao X, Zou D, Zhu C, et al. The synergistic effect of hierarchical micro/nano-topography and bioactive ions for enhanced osseointegration. Biomaterials 2013;34:3184-3195.

45. Gittens RA, Olivares-Navarrete R, Schwartz Z, Boyan BD. Implant osseointegration and the role of microroughness and nanostructures: lessons for spine implants. Acta Biomater 2014;10:3363-3371.

46. Kieswetter K, Schwartz Z, Hummert TW, Cochran DL, Simpson J, Dean DD, et al. Surface roughness modulates the local production of growth factors and cytokines by osteoblast-like MG-63 cells. J Biomed Mater Res 1996;32:55-63.

47. Lossdorfer S, Schwartz Z, Wang L, Lohmann CH, Turner JD, Wieland M, et al. Microrough implant surface topographies increase osteogenesis by reducing osteoclast formation and activity. J Biomed Mater Res A 2004;70:361-369.

48. Olivares-Navarrete R, Hyzy SL, Pan Q, Dunn G, Williams JK, Schwartz Z, et al. Osteoblast maturation on microtextured titanium involves paracrine regulation of bone morphogenetic protein signaling. J Biomed Mater Res A 2015;103:1721-1731.

49. Small W, Buckley PR, Wilson TS, Benett WJ, Hartman J, Saloner D, et al. Shape memory polymer stent with expandable foam: a new concept for endovascular embolization of fusiform aneurysms. IEEE Trans Biomed Eng 2007;54:1157-1160.

50. Ortega J, Maitland D, Wilson T, Tsai W, Savas O, Saloner D. Vascular dynamics of a shape memory polymer foam aneurysm treatment technique. Ann Biomed Eng 2007;35:1870-1884.

51. Navarese EP, Kowalewski M, Cortese B, Kandzari D, Dias S, Wojakowski W, et al. Short and long-term safety and efficacy of polymer-free vs. durable polymer drug-eluting stents. A comprehensive meta-analysis of randomized trials including 6178 patients. Atherosclerosis 2014;233:224-231.

52. Kelch S, Steuer S, Schmidt AM, Lendlein A. Shape-memory polymer networks from oligo[(epsilon-hydroxycaproate)-co-glycolate]dimethacrylates and butyl acrylate with adjustable hydrolytic degradation rate. Biomacromolecules 2007;8:1018-1027.

53. Lu XL, Sun ZJ, Cai W, Gao ZY. Study on the shape memory effects of poly(L-lactide-co-epsilon-caprolactone) biodegradable polymers. J Mater Sci Mater Med 2008;19:395-399.

54. Wong YS, Xiong Y, Venkatraman SS, Boey FY. Shape memory in un-cross-linked biodegradable polymers. J Biomater Sci Polym Ed 2008;19:175-191.

55. Wache HM, Tartakowska DJ, Hentrich A, Wagner MH. Development of a polymer stent with shape memory effect as a drug delivery system. J Mater Sci Mater Med 2003;14:109-112.

56. Song L, Hu W, Zhang H, Wang G, Yang H, Zhu S. In vitro evaluation of chemically cross-linked shape-memory acrylate-methacrylate copolymer networks as ocular implants. J Phys Chem B 2010;114:7172-7178.

57. Turner SA, Zhou J, Sheiko SS, Ashby VS. Switchable micropatterned surface topographies mediated by reversible shape memory. ACS Appl Mater Interfaces 2014;6:8017-8021.

58. Safranski DL, Gall K. Effect of chemical structure and crosslinking density on the thermo-mechanical properties and toughness of (meth)acrylate shape memory polymer networks. Polymer 2008;49:4446.

59. Zhao G, Raines AL, Wieland M, Schwartz Z, Boyan BD. Requirement for both micron- and submicron scale structure for synergistic responses of osteoblasts to substrate surface energy and topography. Biomaterials 2007;28:2821-2829.

60. Le DM, Kulangara K, Adler AF, Leong KW, Ashby VS. Dynamic topographical control of mesenchymal stem cells by culture on responsive poly(epsilon-caprolactone) surfaces. Adv Mater 2011;23:3278-3283.

61. Tseng LF, Mather PT, Henderson JH. Shape-memory-actuated change in scaffold fiber alignment directs stem cell morphology. Acta Biomater 2013;9:8790-8801.

62. Davis KA, Burke KA, Mather PT, Henderson JH. Dynamic cell behavior on shape memory polymer substrates. Biomaterials 2011;32:2285-2293.

63. Neuss S, Blomenkamp I, Stainforth R, Boltersdorf D, Jansen M, Butz N, et al. The use of a shape-memory poly(epsilon-caprolactone)dimethacrylate network as a tissue engineering scaffold. Biomaterials 2009;30:1697-1705.

64. Guvendiren M, Burdick JA. Stem cell response to spatially and temporally displayed and reversible surface topography. Adv Healthc Mater 2013;2:155-164.

65. Xu S, Zhang P, Zhu G, Jiang Y. Effect of biodegradable shape-memory polymers on proliferation of 3T3 cells. J Mater Eng Perform 2011;20:807-811.

66. Bao M, Lou X, Zhou Q, Dong W, Yuan H, Zhang Y. Electrospun biomimetic fibrous Scaffold from shape memory polymer of PDLLA-co-TMC for bone tissue engineering. ACS Appl Mater Interfaces 2014;6:2611–2621.

67. Zhao L, Liu L, Wu Z, Zhang Y, Chu PK. Effects of micropitted/nanotubular titania topographies on bone mesenchymal stem cell osteogenic differentiation. Biomaterials 2012;33:2629-2641.

68. Thorpe SD, Buckley CT, Steward AJ, Kelly DJ. European Society of Biomechanics S.M. Perren Award 2012: The external mechanical environment can override the influence of local substrate in determining stem cell fate. J Biomech 2012;45:2483-2492.

69. Olivares-Navarrete R, Rodil SE, Hyzy SL, Dunn GR, Almaguer-Flores A, Schwartz Z, et al. Role of integrin subunits in mesenchymal stem cell differentiation and osteoblast maturation on graphitic carbon-coated microstructured surfaces. Biomaterials 2015;51:69-79.

70. Olivares-Navarrete R, Raz P, Zhao G, Chen J, Wieland M, Cochran DL, et al. Integrin alpha2beta1 plays a critical role in osteoblast response to micron-scale surface structure and surface energy of titanium substrates. Proc Natl Acad Sci U S A 2008;105:15767-15772.

71. LaPointe VLS, Fernandes AT, Bell NC, Stellacci F, Stevens MM. Nanoscale Topography and Chemistry Affect Embryonic Stem Cell Self-Renewal and Early Differentiation. Advanced Healthcare Materials 2013;2:1644-1650.

72. Low WC, Rujitanaroj P-, Lee D-, Kuang J, Messersmith PB, Chan JKY, et al. Mussel-Inspired Modification of Nanofibers for REST siRNA Delivery: Understanding the Effects of Gene-Silencing and Substrate Topography on Human Mesenchymal Stem Cell Neuronal Commitment. Macromolecular Bioscience 2015;15:1457-1468.

73. Platzman I, Muth CA, Lee-Thedieck C, Pallarola D, Atanasova R, Louban I, et al. Surface properties of nanostructured bio-active interfaces: impacts of surface stiffness and topography on cell–surface interactions. RSC Advances 2013;3:13293.

74. Li Z, Gong Y, Sun S, Du Y, Lu D, Liu X, et al. Differential regulation of stiffness, topography, and dimension of substrates in rat mesenchymal stem cells. Biomaterials 2013;34:7616-7625.

75. Mengsteab PY, Uto K, Smith AS, Frankel S, Fisher E, Nawas Z, et al. Spatiotemporal control of cardiac anisotropy using dynamic nanotopographic cues. Biomaterials 2016;86:1-10.

76. Ebara M, Uto K, Idota N, Hoffman JM, Aoyagi T. The taming of the cell: shape-memory nanopatterns direct cell orientation. Int J Nanomedicine 2014;9 Suppl 1:117-126.

77. Ebara M, Akimoto M, Uto K, Shiba K, Yoshikawa G, Aoyagi T. Focus on the interlude between topographic transition and cell response on shape-memory surfaces. Polymer 2014;55:5961-5968.

78. Davis KA, Henderson JH. 2013 39th Annual Northeast Bioengineering Conference; Dynamic Micropattern Geometry atop Shape Memory Polymers. 2013:33-34.

79. Sharifi S, van Kooten TG, Kranenburg HJ, Meij BP, Behl M, Lendlein A, et al. An annulus fibrosus closure device based on a biodegradable shape-memory polymer network. Biomaterials 2013;34:8105-8113.

80. Bencherif SA, Sands RW, Bhatta D, Arany P, Verbeke CS, Edwards DA, et al. Injectable preformed scaffolds with shape-memory properties. Proc Natl Acad Sci U S A 2012;109:19590-19595.

81. Gong T, Zhao K, Yang G, Li J, Chen Hi, Chen Y, et al. The Control of Mesenchymal Stem Cell Differentiation Using Dynamically Tunable Surface Microgrooves. Adv Healthcare Mater 2014;3:1608-1619.

82. Tseng LF, Wang J, Baker RM, Wang G, Mather PT, Henderson JH. Osteogenic Capacity of Human Adipose-Derived Stem Cells is Preserved Following Triggering of Shape Memory Scaffolds. Tissue Eng Part A 2016;22:1026-1035.

83. De Nardo L, Bertoldi S, Cigada A, Tanzi MC, Haugen HJ, Fare S. Preparation and characterization of shape memory polymer scaffolds via solvent casting/particulate leaching. J Appl Biomater Funct Mater 2012;10:119-126.

84. Baker RM, Yang P, Henderson JH, Mather PT. 2011 IEEE 37th Annual Northeast Bioengineering Conference (NEBEC); Wrinkle formation on a biocompatible shape memory polymer. 2011:1-2.

85. Xing J, Ma Y, Lin M, Wang Y, Pan H, Ruan C, et al. Stretching-induced nanostructures on shape memory polyurethane films and their regulation to osteoblasts morphology. Colloids Surf B Biointerfaces 2016;146:431-441.

86. Chun YW, Khang D, Haberstroh KM, Webster TJ. The role of polymer nanosurface roughness and submicron pores in improving bladder urothelial cell density and inhibiting calcium oxalate stone formation. Nanotechnology 2009;20:085104.

87. Dueramae I, Nishida M, Nakaji-Hirabayashi T, Matsumura K, Kitano H. Biodegradable shape memory polymers functionalized with anti-biofouling interpenetrating polymer networks. J.Mater.Chem.B 2016;4:5394 5404.

88. Bao M, Wang X, Yuan H, Lou X, Zhao Q, Zhang Y. HAp incorporated ultrafine polymeric fibers with shape memory effect for potential use in bone screw hole healing. J.Mater.Chem.B 2016;4:5308 5320.

89. Shao Z, Zhang X, Pi Y, Wang X, Jia Z, Zhu J, et al. Polycaprolactone electrospun mesh conjugated with an MSC affinity peptide for MSC homing in vivo. Biomaterials 2012;33:3375-3387.

90. Michel M, Dahmann C. Memorizing Shape to Orient Cell Division. Dev Cell 2016;36:589-590.

91. Brunetti V, Maiorano G, Rizzello L, Sorce B, Sabella S, Cingolani R, et al. Neurons sense nanoscale roughness with nanometer sensitivity. Proc Natl Acad Sci U S A 2010;107:6264-6269.

92. Lüthen F, Lange R, Becker P, Rychly J, Beck U, Nebe JGB. The influence of surface roughness of titanium on ß1- and ß3-integrin adhesion and the organization of fibronectin in human osteoblastic cells. Biomaterials 2005;26:2423-2440.

93. Geblinger D, Addadi L, Geiger B. Nano-topography sensing by osteoclasts. J Cell Sci 2010;123:1503-1510.

94. Chuah YJ, Zhang Y, Wu Y, Menon NV, Goh GH, Lee AC, et al. Combinatorial effect of substratum properties on mesenchymal stem cell sheet engineering and subsequent multi-lineage differentiation. Acta Biomater 2015;23:52-62.

95. Torres FG, Troncoso OP, Gamucci O, Corvaglia S, Brunetti V, Bardi G. Immunological properties of Andean starch films are independent of their nanometric roughness and stiffness. Int J Biol Macromol 2015;75:460-466.

96. The Eleven Most Implanted Medical Devices In America - 24/7 Wall St. ;2014.

97. Nava MM, Raimondi MT, Pietrabissa R. Controlling self-renewal and differentiation of stem cells via mechanical cues. J Biomed Biotechnol 2012;2012:797410.

98. Rehfeldt F, Engler AJ, Eckhardt A, Ahmed F, Discher DE. Cell responses to the mechanochemical microenvironment--implications for regenerative medicine and drug delivery. Adv Drug Deliv Rev 2007;59:1329-1339.

99. Reilly GC, Engler AJ. Intrinsic extracellular matrix properties regulate stem cell differentiation. J Biomech 2010;43:55-62.

100. Sanz-Ramos P, Mora G, Ripalda P, Vicente-Pascual M, Izal-Azcarate I. Identification of signalling pathways triggered by changes in the mechanical environment in rat chondrocytes. Osteoarthritis Cartilage 2012;20:931-939.

101. Seib FP, Prewitz M, Werner C, Bornhauser M. Matrix elasticity regulates the secretory profile of human bone marrow-derived multipotent mesenchymal stromal cells (MSCs). Biochem Biophys Res Commun 2009;389:663-667.

102. Xue R, Li JY, Yeh Y, Yang L, Chien S. Effects of matrix elasticity and cell density on human mesenchymal stem cells differentiation. J Orthop Res 2013;31:1360-1365.

103. Her GJ, Wu HC, Chen MH, Chen MY, Chang SC, Wang TW. Control of three-dimensional substrate stiffness to manipulate mesenchymal stem cell fate toward neuronal or glial lineages. Acta Biomater 2013;9:5170-5180.

104. Angele P, Muller R, Schumann D, Englert C, Zellner J, Johnstone B, et al. Characterization of esterified hyaluronan-gelatin polymer composites suitable for chondrogenic differentiation of mesenchymal stem cells. J Biomed Mater Res A 2009;91:416-427.

105. Calvo-Guirado JL, Gomez Moreno G, Aguilar-Salvatierra A, Mate Sanchez de Val JE, Abboud M, Nemcovsky CE. Bone remodeling at implants with different configurations and placed immediately at different depth into extraction sockets. Experimental study in dogs. Clin Oral Implants Res 2015;26:507-515.

106. Sartoretto SC, Alves AT, Resende RF, Calasans-Maia J, Granjeiro JM, Calasans-Maia MD. Early osseointegration driven by the surface chemistry and wettability of dental implants. J Appl Oral Sci 2015;23:279-287.

107. Lee HJ, Yang IH, Kim SK, Yeo IS, Kwon TK. In vivo comparison between the effects of chemically modified hydrophilic and anodically oxidized titanium surfaces on initial bone healing. J Periodontal Implant Sci 2015;45:94-100.

108. Munoz-Pinto DJ, Jimenez-Vergara AC, Hou Y, Hayenga HN, Rivas A, Grunlan M, et al. Osteogenic potential of poly(ethylene glycol)-poly(dimethylsiloxane) hybrid hydrogels. Tissue Eng Part A 2012;18:1710-1719.

109. Marletta G, Ciapetti G, Satriano C, Perut F, Salerno M, Baldini N. Improved osteogenic differentiation of human marrow stromal cells cultured on ion-induced chemically structured poly-e-caprolactone. Biomaterials 2007;28:1132 1140.

110. Wang JR, Ahmed SF, Gadegaard N, Meek RM, Dalby MJ, Yarwood SJ. Nanotopology potentiates growth hormone signalling and osteogenesis of mesenchymal stem cells. Growth Horm IGF Res 2014;24:245-250.

111. Olivares-Navarrete R, Hyzy SL, Hutton DL, Erdman CP, Wieland M, Boyan BD, et al. Direct and indirect effects of microstructured titanium substrates on the induction of mesenchymal stem cell differentiation towards the osteoblast lineage. Biomaterials 2010;31:2728-2735.

112. Keselowsky BG, Wang L, Schwartz Z, Garcia AJ, Boyan BD. Integrin alpha(5) controls osteoblastic proliferation and differentiation responses to titanium substrates presenting different roughness characteristics in a roughness independent manner. J Biomed Mater Res A 2007;80:700-710.

113. Moore SW, Roca-Cusachs P, Sheetz MP. Stretchy proteins on stretchy substrates: the important elements of integrin-mediated rigidity sensing. Dev Cell 2010;19:194-206.

114. Du J, Chen X, Liang X, Zhang G, Xu J, He L, et al. Integrin activation and internalization on soft ECM as a mechanism of induction of stem cell differentiation by ECM elasticity. Proc Natl Acad Sci U S A 2011;108:9466-9471.

115. Steward AJ, Wagner DR, Kelly DJ. The pericellular environment regulates cytoskeletal development and the differentiation of mesenchymal stem cells and determines their response to hydrostatic pressure. Eur Cell Mater 2013;25:167-178.

116. Loeser RF, Carlson CS, McGee MP. Expression of ß1 Integrins by Cultured Articular Chondrocytes and in Osteoarthritic Cartilage. Exp Cell Res 1995;217:248 257.

117. Enomoto M, Leboy PS, Menko AS, Boettiger D. ß1 Integrins Mediate Chondrocyte Interaction with Type I Collagen, Type II Collagen, and Fibronectin. Exp Cell Res 1993;205:276-285.

118. Engel FE, Khare AG, Boyan BD. Phenotypic changes of rabbit mandibular condylar cartilage cells in culture. J Dent Res 1990;69:1753-1758.

119. Kitaoka E, Satomura K, Hayashi E, Yamanouchi K, Tobiume S, Kume K, et al. Establishment and characterization of chondrocyte cell lines from the costal cartilage of SV40 large T antigen transgenic mice. J Cell Biochem 2001;81:571-582.

120. Li X, Huang Y, Zheng L, Liu H, Niu X, Huang J, et al. Effect of substrate stiffness on the functions of rat bone marrow and adipose tissue derived mesenchymal stem cells in vitro. J Biomed Mater Res A 2014;102:1092-1101.

121. Park JS, Chu JS, Tsou AD, Diop R, Tang Z, Wang A, et al. The effect of matrix stiffness on the differentiation of mesenchymal stem cells in response to TGF-beta. Biomaterials 2011;32:3921-3930.

122. Bayati V, Altomare L, Tanzi MC, Fare S. Adipose-derived stem cells could sense the nano-scale cues as myogenic-differentiating factors. J Mater Sci Mater Med 2013;24:2439-2447.

123. Genes NG, Rowley JA, Mooney DJ, Bonassar LJ. Effect of substrate mechanics on chondrocyte adhesion to modified alginate surfaces. Arch Biochem Biophys 2004;422:161-167.

124. Huebsch N, Arany PR, Mao AS, Shvartsman D, Ali OA, Bencherif SA, et al. Harnessing traction-mediated manipulation of the cell/matrix interface to control stem-cell fate. Nat Mater 2010;9:518-526.

125. Sun J, Zhou H, Deng Y, Zhang Y, Gu P, Ge S, et al. Conditioned medium from bone marrow mesenchymal stem cells transiently retards osteoblast differentiation by downregulating runx2. Cells Tissues Organs 2012;196:510-522.

126. Lee KS, Kim HJ, Li QL, Chi XZ, Ueta C, Komori T, et al. Runx2 Is a Common Target of Transforming Growth Factor ß1 and Bone Morphogenetic Protein 2, and Cooperation between Runx2 and Smad5 Induces Osteoblast-Specific Gene Expression in the Pluripotent Mesenchymal Precursor Cell Line C2C12. Mol Cell Bio 2000;20:8783-8792.

127. Dieudonne FX, Severe N, Biosse-Duplan M, Weng JJ, Su Y, Marie PJ. Promotion of osteoblast differentiation in mesenchymal cells through Cbl-mediated control of STAT5 activity. Stem Cells 2013;31:1340-1349.

128. Alexopoulos LG, Williams GM, Upton ML, Setton LA, Guilak F. Osteoarthritic changes in the biphasic mechanical properties of the chondrocyte pericellular matrix in articular cartilage. J Biomech 2005;38:509 517.

129. Willems NM, Langenbach GE, Stoop R, den Toonder JM, Mulder L, Zentner A, et al. Higher number of pentosidine cross-links induced by ribose does not alter tissue stiffness of cancellous bone. Mater Sci Eng C Mater Biol Appl 2014;42:15-21.

130. Vater C, Kasten P, Stiehler M. Culture media for the differentiation of mesenchymal stromal cells. Acta Biomater 2011;7:463-477.

131. Murphy CM, Matsiko A, Haugh MG, Gleeson JP, O'Brien FJ. Mesenchymal stem cell fate is regulated by the composition and mechanical properties of collagen-glycosaminoglycan scaffolds. J Mech Behav Biomed Mater 2012;11:53-62.

132. Witkowska-Zimny M, Walenko K, Walkiewicz AE, Pojda Z, Przybylski J, Lewandowska-Szumiel M. Effect of substrate stiffness on differentiation of umbilical cord stem cells. Acta Biochim Pol 2012;59:261-264.

133. Chandler EM, Berglund CM, Lee JS, Polacheck WJ, Gleghorn JP, Kirby BJ, et al. Stiffness of photocrosslinked RGD-alginate gels regulates adipose progenitor cell behavior. Biotechnol Bioeng 2011;108:1683-1692.

134. Darling EM, Wilusz RE, Bolognesi MP, Zauscher S, Guilak F. Spatial mapping of the biomechanical properties of the pericellular matrix of articular cartilage measured in situ via atomic force microscopy. Biophys J 2010;98:2848-2856.

135. Shih YR, Tseng KF, Lai HY, Lin CH, Lee OK. Matrix stiffness regulation of integrin-mediated mechanotransduction during osteogenic differentiation of human mesenchymal stem cells. J Bone Miner Res 2011;26:730-738.

136. Yeung T, Georges PC, Flanagan LA, Marg B, Ortiz M, Funaki M, et al. Effects of substrate stiffness on cell morphology, cytoskeletal structure, and adhesion. Cell Motil Cytoskeleton 2005;60:24-34.

137. Frith JE, Mills RJ, Hudson JE, Cooper-White JJ. Tailored integrin-extracellular matrix interactions to direct human mesenchymal stem cell differentiation. Stem Cells Dev 2012;21:2442-2456.

138. Bougault C, Cueru L, Bariller J, Malbouyres M, Paumier A, Aszodi A, et al. Alteration of cartilage mechanical properties in absence of beta1 integrins revealed by rheometry and FRAP analyses. J Biomech 2013;46:1633-1640.

# VITA

## ERIN M. LEE

LEE was born in Springfield, Oregon. She attended public schools in Portland, Oregon, received an honors B.A. in Bioengineering from Oregon Statue University, Corvallis, Oregon in 2004, and worked for a number of years in youth ministry before coming to Georgia Tech to pursue a doctorate in Biomedical Engineering. When not spending copious amounts of hours in the lab, Mrs. Lee enjoys reading, hiking, white water rafting, ziplining, and relaxing with her husband John.